AD-A158 234 RESEARCH ON INTENSE ELECTRON BEAMS AND APPLICATIONS(U) 1/1
BERKELEY RESEARCH ASSOCIATES INC CA JUL 84
PD-BRA-84-317R N00014-83-C-2157

UNCLASSIFIED F/G 20/7 NL

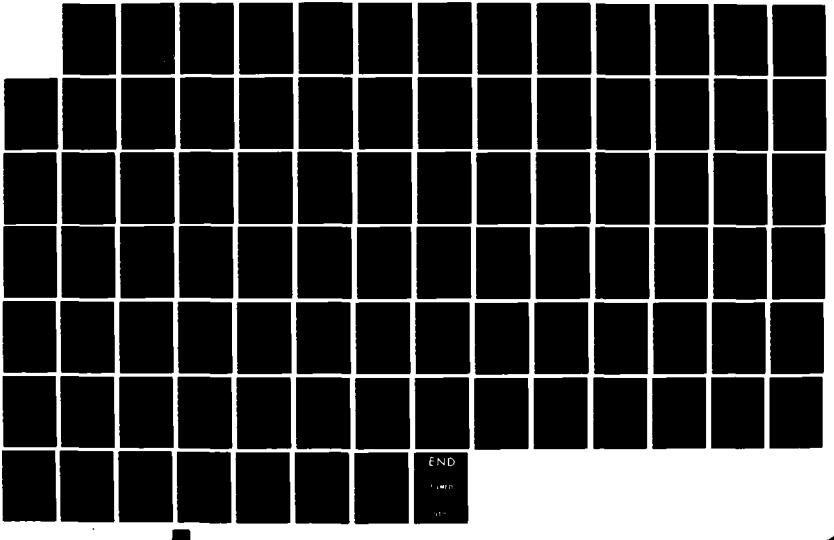

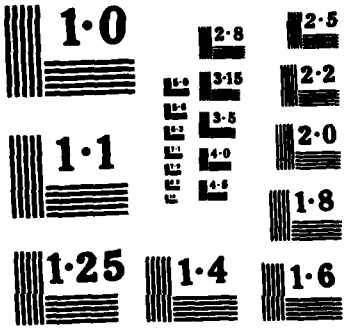

NATIONAL BUREAU OF STANDARDS
MICROCOPY RESOLUTION TEST CHART

PD-BRA-84-317R
July 1984

RESEARCH ON INTENSE ELECTRON BEAMS AND APPLICATIONS

Final Report
Contract N00014-83-C-2157

for
Plasma Physics Division
Naval Research Laboratory

by
Berkeley Research Associates
P.O. Box 241
Berkeley, California 94701

TABLE OF CONTENTS

I. INTRODUCTION

This report discusses research carried out by Berkeley Research Associates, Inc. under contract #N00014-83-C-2157 with the Plasma Physics Division of the Naval Research Laboratory. The report covers the performance period 1 May 1983 to 30 April 1984. During this period, an extensive investigation of electron beam stability was carried out in the context of an easily formulated 2-D cold electron layer model. This work was carried on in close association with NRL personnel in conjunction with the special focus program, "Advanced Accelerators."

The modified betatron has been the subject of an intense investigation by NRL staff as a potential high current electron accelerator. Significant progress has been made in the understanding of the operation of this device and a large experimental effort designed to test this understanding is now well underway. Much of the work to date has been directed toward a formulation of the in situ beam dynamics, involving equilibrium [1,2,3] and stability [4,5,6] considerations, while other research has been directed toward solving the difficult injection problem [7,8].

Once an equilibrium is established, which in general requires constraints on beam density and on the betatron field index, stability questions of two general types arise. First is the question of the stability of the betatron

oscillations in the presence of small field errors, i.e. the problem of orbital resonances. These resonances are basically single particle effects caused by a repeated in-phase interaction of a particle with a field imperfection. However, even though they are basically single particle effects, resonances can set a limit to the beam current in an accelerator since the betatron frequency of one particle is affected by the collective fields of the other particles in the beam. These resonant instabilities were studied under an earlier contract with NRL, N00014-81-C-2371.

The second broad class of instabilities occurs in a device with "perfect" (azimuthally symmetric) applied fields. These generally come under the heading of collective effects and include the various mechanisms by which the beam may bunch, kink, or simply spiral toward the chamber wall. They include the negative-mass-kink mode and the various resistive wall instabilities, all of which place certain constraints on beam current.

The various collective instabilities in the modified betatron were first studied by Sprangle and Vomvoridis[5], who characterized the different modes and analyzed the dependence of the growth rates on system parameters. Building on this work, Sprangle and Chernin[9] investigated, under somewhat more general conditions, the behavior of the growth rates as current was raised, keeping the beam energy spread fixed.

A rather unusual and unexpected result was found, namely, a double-valuedness in the current versus energy spread stability curve and the appearance of two disjoint stability regions. This double-valuedness was attributed to the effects of self fields and was found to be the result of a competition between the growth and stabilization mechanisms. Under some conditions, the double valuedness could even be present for a conventional betatron configuration.

Prompted by this novel finding and mindful that the three-dimensional nature of the problem made inclusion of self field effects necessarily approximate, a rigorous study was begun of a two-dimensional model, including correctly the crucial radial and azimuthal particle dynamics, but neglecting the inessential dynamics in the axial direction. This model has the advantage that all self field effects could be included exactly in the formulation of the eigenvalue problem governing the small signal behavior. This study quickly developed in several interesting directions, having now produced potentially useful results for beam behavior in accelerators, storage rings, and microwave tubes. It is the results of this study which are reported here.

The following section describes the model we have used, discusses its essential features, and summarizes our findings. Detailed analysis is given in papers attached as Appendices. Also included as an Appendix is documentation

and a listing of a computer code developed under this contract which locates the eigenvalues for the stability problem for the case of perfectly conducting chamber walls. A final section suggests directions for future work.

II. TWO-DIMENSIONAL LAMINAR ELECTRON LAYER MODEL

The negative mass instability, diocotron instability, and electron cyclotron maser instability all depend in some way on the existence of shear in the fluid velocity in the underlying equilibrium state. Self fields in an intense beam may affect the magnitude and even the sign of the shear in a beam; hence it is important to include self field effects accurately in any analysis of these beam instabilities.

The cold fluid equilibria in a torus are quite difficult to calculate[3]. The stability analysis is even more involved. To make progress, certain simplifying assumptions about the functional form of the self fields are often made[5]. These assumptions may affect the dependence of the shear on the beam density. One is therefore motivated to consider a "beam" model which retains the important effects of curvature while allowing an exact treatment of self field effects. Such a model--the E-layer or Astron model--is illustrated in Figure 1. Here a laminar layer of electrons is supported by a combination of radial electric and axial magnetic fields between two coaxial cylinders. Here the cylinders will be taken to be perfect conductors, though resistive wall and other boundary effects may be included in a straightforward way, as discussed in Appendix B.

The E-layer model has been the subject of numerous studies[10-12]. Surprisingly, however, the exact linear

stability analysis for a finite thickness, relativistic layer does not seem to have been carried out previously. so, perhaps as a consequence, some very interesting, potentially useful features of the model appear to have been missed and the unifying relationships[13] among the various instabilities seem not to be widely appreciated.

In the basic equilibrium state illustrated in Figure 1, only a radial electric field (E_r) and an axial magnetic field (B_z) exist. These fields are in general due to a combination of self and applied fields. The equilibrium is governed by the following set of three equations (MKS units):

$$\frac{\gamma_o v_o^2}{r} = \frac{e}{m} [E_o + v_o B_o] \tag{1}$$

$$\frac{1}{r} \frac{d}{dr}(rE_o) = -en_o/\varepsilon_o \tag{2}$$

$$\frac{dB_o}{dr} = \mu_o e n_o v_o \quad . \tag{3}$$

These equations must be solved subject to a specified potential difference between the inner and outer walls and specified total magnetic flux. A method for doing this and some features of the solution are discussed in Section II of Appendix B. Here we note only that solutions may be generally grouped into three types, depending on which two of the three terms in the equation of force balance, Eq. (1), are most important. The three cases are: (I) magnetic force

balances centrifugal force (e.g. Astron, gyrotron, particle accelerators), (II) electric force balances magnetic force (e.g. crossed field microwave devices), and (III) electric force balances centrifugal force (e.g. orbitron[14], heliotron[15]). Our analysis, therefore, has wide applicability and many standard results may be recovered in appropriate limits, as discussed in Appendix B.

One of the most important equilibrium quantities is the dependence of the rotation frequency $\omega_o \equiv v_o/r$ on the energy $E \equiv mc^2\gamma - e\phi$. This quantity may be shown to be given by

$$\frac{d\omega_o}{dE} = -\frac{\omega_o}{mc^2\gamma_o\beta_o^2}\left[\frac{\beta_o^2+2h+\xi/\gamma_o^4}{1+\gamma_o^2h^2-\xi/\gamma_o^2}\right] \tag{4}$$

where $\xi = \omega_p^2/\omega_o^2$, ω_p is the plasma frequency, and

$$h = \frac{erE_o}{mc^2\beta_o^2\gamma_o^3} \quad . \tag{5}$$

When ω_o is a decreasing function of energy, one expects the usual negative mass instability mechanism to operate. However, we note the possibility of reversing the sign of $d\omega_o/dE$ by judicious choice of applied electric field. In fact, as detailed analysis shows, the negative mass instability may be completely stabilized by choosing $\beta_o^2 + 2h < 0$. A discussion of this result is given in Appendix A and a detailed derivation in Appendix B. Another noteworthy feature of Eq. (4) is that it possesses a (negative) extremum

as a function of h, at $h = \gamma_o^{-2}$. Since $h\gamma_o^2$ is the ratio of electric to centrifugal forces we identify those devices of Type III as the most unstable type of microwave generators. This result suggests that the orbitron and heliotron might possess some advantages over other microwave tubes. This possibility is presently under investigation.

The linear stability of equilibria described by Eqs. (1-3) to perturbations in the r and θ directions has been studied in some detail. The eigenvalue problem for the TE modes has the form

$$r\frac{d}{dr}(r\tilde{A}\frac{d\phi}{dr}) + \tilde{C}\phi = 0 \qquad (6)$$

where $\phi = rE_{\theta 1}$ and where $\tilde{A}$ and $\tilde{C}$ are complicated functions or r, the azimuthal mode number ℓ, and the eigenvalue ω. The full equation is derived in Appendix B where the features of the equation are also discussed. We emphasize that Eq. (6) is fully relativistic, fully electromagnetic, and contains all effects of self fields.

Eq. (6) describes two basic unstable modes, the longitudinal mode, satisfying $\omega - \ell\omega_o \simeq 0$ and the transverse mode, for which $\omega - \ell\omega_o \simeq \pm \omega_o(1 + \gamma_o^2 h^2)^{\frac{1}{2}}$. The longitudinal mode involves significant azimuthal bunching while the transverse mode involves mostly radial motion of the layer. In the planar limit, it may be shown that the transverse mode reduces to the so-called Buneman instability[16], first studied in connection with the early magnetrons. In cylindrical

geometry the transverse mode has been invoked to explain the operation of the peniotron[17].

Our studies have been concentrated on the longitudinal mode which includes the negative mass, cyclotron maser, and diocotron instabilities. For a thin layer it is possible to obtain an analytical approximation to the growth rate for the longitudinal mode, as shown in Appendix B:

$$[\mathrm{Im}(\omega)]^2 = \frac{\ell \frac{\tau}{R} \omega_p^2}{(b_+ + b_-)} \frac{(\beta_o^2 + 2h)}{(1+\gamma_o^2 h^2)} + O(\ell\tau/R)^2 \qquad (7)$$

where τ = layer thickness, R = layer radius, $b_\pm$ = wave admittances. (See Appendix B, where the second order term is also given explicitly.) This expression for the growth rate has several important features: The growth rate (1) scales as $(\text{current})^{\frac{1}{2}}$; (2) vanishes when $\beta_o^2 + 2h < 0$; (3) has a maximum as a function of h when $h\gamma_o^2 = 1$; and (4) vanishes in the planar limit. Features (2) - (4) are novel findings. They are expected on physical grounds, yet they have not been previously discussed in the literature. Item (2) may have application to low energy (~MeV) storage rings[18]. Note that self field effects were included in the derivation of Eq. (7). The stability condition, (2), therefore, is insensitive to beam current, azimuthal mode number, or container geometry.

Extensive numerical tests of Eq. (7) have been carried out, using a computer code developed to solve Eq. (6) through using a "shooting method." In the tests all parameters but one

were held fixed and the dependence of the growth rate on the single variable parameter was determined and compared with Eq. (7). The parameters tested were h, ν/γ_o, τ/R, b/R, a/R, γ_o, and ℓ. Good agreement was found in all cases; details are given in Appendix B. The computer code used to solve the eigenvalue problem is documented in Appendix C.

In addition to these tests, a search was carried out for evidence of the double valuedness in the current vs. energy spread curve, the prediction of which was the original motivation for this work. Despite much effort, no such double valuedness was uncovered. The search is complicated, however, because it is difficult to develop a set of parameters for layers with the same energy spread, but different currents since, for large currents, the energy spread is a function of the current. In fact, current, energy spread, and beam thickness are connected in a way that is absent in the equilibrium used in reference 9. The reason is that in reference 9, betatron oscillations are assumed to "fill in" the beam to the size and shape assumed when calculating the self fields. Inclusion of betatron oscillations in the E-layer model may help to carry out an effective comparison more readily, but this is not easily done. A definitive resolution of the question on the existence of double-valuedness must await further analysis, though numerical particle simulations may also be helpful in shedding some light on this question.

III. SUMMARY AND RECOMMENDATIONS

A detailed study of a two-dimensional electron layer confined between coaxial cylinders has been carried out with the intention of understanding the radial and azimuthal beam dynamics in high current accelerators. Though no confirmation could be found for the predicted[9] double-valuedness in the current versus energy spread curve, several interesting and potentially useful features of electron beam behavior in curved geometries were discovered. Specifically, it was found that by appropriate choices of applied electric field, the growth rate of the longitudinal mode could either be maximized, as might be desirable in certain microwave devices, or eliminated altogether, as would be desirable in electron accelerators and storage rings. In addition, a long-standing puzzle concerning the survival of a finite growth rate for the negative mass instability in the planar limit was resolved.

There are several areas where further work would be useful. First, additional research is needed to resolve the question of double valuedness discussed above. The problem is a difficult one, however, and computer simulations may be needed to resolve this complex issue. Second, the effects on beam behavior of other applied magnetic or electric fields is also an important area for further investigation. In particular, inclusion of a toroidal field in the

E-layer model is straightforward and leads to a fourth order eigenvalue problem whose features are important to study. Careful examination of this problem may lead to a more thorough understanding of the effect of the toroidal field on beam stability in the modified betatron. And finally, we mention that the effect of strong focusing fields on these instabilities is an important topic for future study, since it has been shown that use of such fields may have certain beneficial effects on the beam behavior. Even these fields may be included in the E-layer model if θ-dependence is allowed in the equilibrium state.

REFERENCES

1. D. Chernin and P. Sprangle, Part. Accelerators 12, 85 (1982).
2. C.A. Kapetanakos, et. al., Phys. Fluids 26, 1634 (1983).
3. J.M. Finn and W.M. Manheimer, Phys. Fluids 26, 3400 (1983).
4. D. Chernin and P. Sprangle, Part. Accelerators 12, 101 (1982).
5. P. Sprangle and J.M. Vomvoridis, NRL Memorandum Report 4688.
6. W.M. Manheimer, Part. Accelerators 13, 209 (1983).
7. C.A. Kapetanakos, P. Sprangle, and S.J. Marsh, NRL Memorandum Report 4835.
8. F. Mako et. al., NRL Memorandum Report 5196.
9. P. Sprangle and D. Chernin, Part. Accelerators (in press).
10. R.H. Levy, Phys. Fluids 8, 1288 (1965).
11. R.J. Briggs and V.K. Neil, Plasma Phys. 9, 209 (1967).
12. D. Chernin and Y.Y. Lau, to be published in Phys. Fluids (and references cited therein).
13. Y.Y. Lau, IEEE Trans. Electron Devices, ED-31, 329 (1984).
14. I. Alexeff and F. Dyer, Phys. Rev. Lett. 43, 351 (1980).
15. R.H. Pantell, IRE Trans. Electron Devices ED-7, 22 (1960).
16. O. Buneman, J. Electron. Control 3, 1,507 (1957).
17. G. Döhler, submitted to IEEE Trans. Electron Devices.
18. Y.Y. Lau and D. Chernin, Phys. Rev. Lett. 52, 1425 (1984).

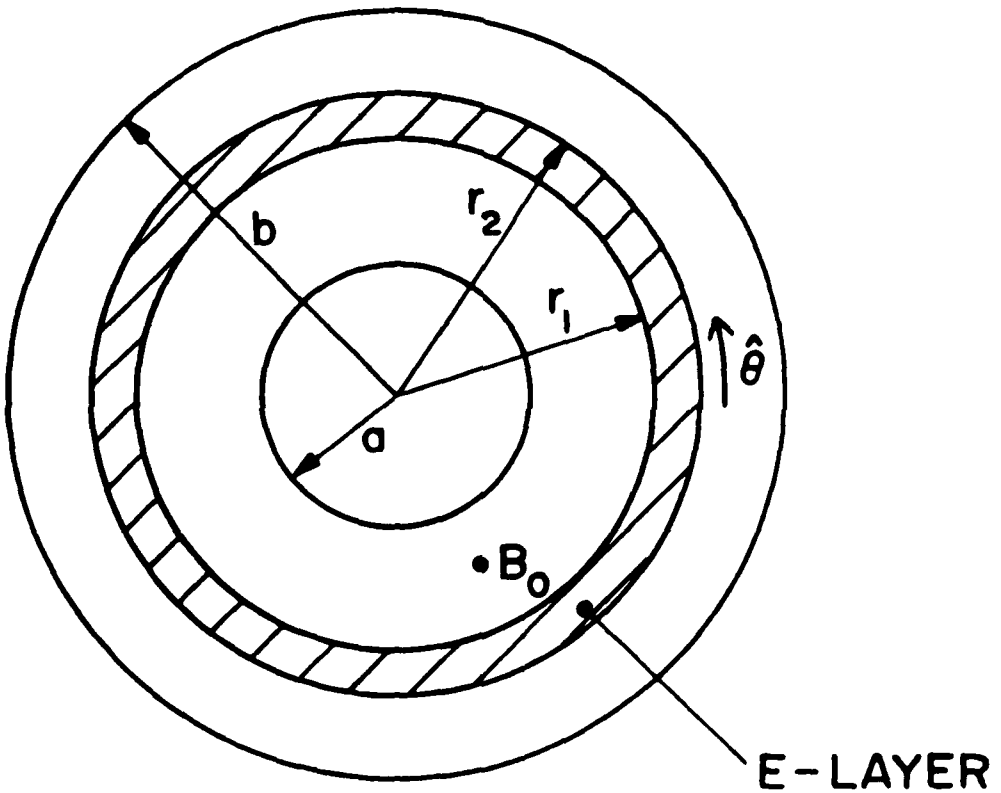

FIGURE 1. The E-Layer or Astron Model

APPENDIX A

Stabilization of the Negative Mass Instability in a Rotating Relativistic Electron Beam

Y.Y. Lau and D. Chernin

Stabilization of the Negative Mass Instability in a Rotating Relativistic Electron Beam

Y. Y. Lau and D. Chernin[a]

Plasma Theory Branch, Plasma Physics Division, Naval Research Laboratory, Washington, D. C. 20375

(Received 9 December 1983)

It is shown that the negative mass instability in a rotating relativistic electron layer may be stabilized by a radial dc electric field of a suitable magnitude. The stabilization mechanism is independent of the beam velocity spread, and is insensitive to the beam current, the container geometry, or the azimuthal mode number. A simple stability criterion is given.

PACS numbers 52.60+h, 29.20-c, 47.75+f, 52.35.Py

The negative mass instability[1] poses a major obstacle to the development of high-current cyclic accelerators. Various methods of stabilization have been proposed and analyzed. Notably, the effects of a moderate beam angular velocity spread and betatron oscillations have been considered.[2-6] For a betatron, the addition of a toroidal magnetic field[7] has been shown to reduce the instability growth rate considerably[5,6] and for the Astron, the proximity of the container walls to the relativistic electron layer (E layer) stabilizes the lower azimuthal modes.[8]

In this Letter, we show that by imposing a negatively biased radial electric field of a suitable strength, the negative mass instability may be suppressed. This stabilization differs from all previously known mechanisms in that it is effective even for a very cold beam; it does not require a toroidal magnetic field, nor is it sensitive to the container geometry, the beam current, or the toroidal mode number. The simple stability criterion, given in Eq. (10) below, does not seem to be very stringent for electron beams in the megaelectronvolt range.

Our finding is based on an analytic treatment of the stability of the E layer situated in a configuration similar to the Astron, which has been shown[8] to include all essential features of the negative mass instability. We limit our study to a highly ordered beam whose unperturbed orbits are concentric circles. Such a beam should yield the most pessimistic prediction as far as the beam stability is concerned; *hence our analysis is conservative*. The simplicity of the assumed equilibrium orbits allows the linear stability theory to be formulated *exactly*, including *all* ac and dc space-charge effects, *all* relativistic effects, and *all* electromagnetic effects, for general equilibrium profiles. As we shall see, our dispersion relation reproduces the standard results in the appropriate limits. For example, the diocotron instability is recovered, and the negative mass instability removed, in the planar, nonrelativistic limit.

Consider a cylindrical E layer with radial density profile $n_0(r)$ which, in equilibrium, circulates concentrically with azimuthal velocity $\bar{v}_0(r) = \hat{\theta} v_0(r) = \hat{\theta} r \omega_0(r)$ under the combined action of an axial magnetic field $\bar{B}_0 = \hat{z} B_0(r)$ and radial electric field $\bar{E}_0 = \hat{r} E_0(r)$. These fields include both the self-fields and the externally imposed fields. We assume that the E layer is located between two cylindrical conductors of inner and outer radii a and b, respectively, and that there is no axial motion nor axial variation in either the unperturbed or the perturbed states.

The governing equations for the equilibrium read

$$\gamma_0 v_0^2/r = -(e/m_0)(E_0 + v_0 B_0), \tag{1}$$

$$dB_0/dr = -\mu_0 J_0 = -\mu_0 e n_0 v_0, \tag{2}$$

$$r^{-1} d(rE_0)/dr = n_0 e/\epsilon_0. \tag{3}$$

Here, e and m_0 are respectively the electron charge and rest mass, μ_0 and ϵ_0 are the free-space permeability and permittivity, and $\gamma_0 = (1 - v_0^2/c^2)^{-1/2}$ is the relativistic mass factor with c being the speed of light. Once the electron density $n_0(r)$, the total electrostatic potential difference between $r = a$ and $r = b$, and the magnetic flux are specified, the unperturbed fields $v_0(r)$, $E_0(r)$, and $B_0(r)$ are to be solved from (1) to (3) to yield a self-consistent equilibrium solution.

We next consider a small-signal perturbation on such an equilibrium. All perturbations are assumed to vary as $f(r)\exp(i\omega t - il\theta)$, where l is the azimuthal mode number and ω is the (complex) eigenfrequency to be determined. In the absence of axial variation and of axial motion, the TM modes and the TE modes are decoupled. The nontrivial components of the rf electromagnetic fields are E_r, E_θ, and B_z for the TE modes. The Maxwell equations, the Lorentz force law, and the continuity equation may then be linearized and combined to yield the following second-order ordinary differential equa-

tion for $\phi = rE_\theta$:

$$\frac{d}{dr}\left[\frac{1}{r\rho}\left[1+\frac{N_D}{\gamma_0^2}\right]\frac{d\phi}{dr}\right]+\phi\left[\frac{\omega_0}{\Omega}\frac{\omega^2}{c^2}\frac{d\eta_D}{dr}+\frac{dA}{dr}+B\right]=0. \tag{4}$$

In this equation

$$\Omega=\omega-l\omega_0(r),\quad N_D=\omega_p^2/\omega_0^2D,\quad \rho=1-l^2c^2/\omega^2r^2+N_D\Omega^2/\omega^2,$$

$$\omega_p^2=e^2n_0/\gamma_0m_0\epsilon_0,\quad D=PQ-\Omega^2/\omega_0^2,\quad P=\gamma_0^2(1+h),\quad Q=h+v_0'/\omega_0,$$

$$\eta_D=N_D(\omega_0/\omega)P/\gamma_0^2,\quad A=-\eta_D(l/\rho r^2)(1+N_D\beta_0^2\Omega/l\omega_0),$$

$$\beta_0=v_0/c,\quad B=(\omega^2/c^2r)(1-\eta_D^2/\rho+N_D/\gamma_0^2).$$

In the definition of Q, a prime denotes a derivative with respect to r, and h is proportional to the equilibrium electric field and is defined by

$$h=-erE_0/m_0\gamma_0^3v_0^2. \tag{5}$$

Note that h is positive (negative) if the equilibrium electric field points radially outward (inward). The eigenvalue ω is determined by solving (4) subject to the boundary conditions $\phi=0$ at $r=a$ and at $r=b$.

Equation (4) is completely general and of wide applicability. It governs the small-signal stability properties of various devices including the Astron,[3,4,8,9] gyrotron,[10] orbitron,[11] and cross-field microwave devices,[12] depending on the parameters of the electron beam as long as the equilibrium states are modeled by Eqs. (1)–(3). A detailed comparative stability study of various types of equilibrium will be given elsewhere. For the present purpose, we restrict ourselves to an E layer with uniform density n_0 extending from $r=r_1$ to $r=r_2$. The E-layer thickness $\tau=r_2-r_1$ is assumed to be much less than the mean radius R. We shall use τ/R as an expansion parameter. Furthermore, we assume that $|\Omega|\ll\omega_0$, a condition readily satisfied by the negative mass mode.[1-10]

The instability growth rate ω_i may be analytically derived from Eq. (4) for a thin E layer by expanding about the singularity $\Omega=0$ in the complex r plane. To two orders in τ/R, it is given by

$$\omega_i^2=\left[\frac{1}{b_++b_-}\right]\omega_p^2\left[\frac{l\tau}{R}\right]\frac{(\beta_0^2+2h)}{(1+\gamma_0^2h^2)}+\frac{l^2\tau^2}{R^2}\Lambda\omega_0^2, \tag{6}$$

where b_+ (b_-) is the normalized wave admittance at the outer (inner) edge of the E layer,[13] and

$$\Lambda=\frac{1}{4}\frac{1}{\gamma_0^6(1+h)^2(1+\gamma_0^2h^2)}$$
$$\times\left\{\left[\frac{\omega_p^2}{\omega_0^2}\right]^2[\beta_0^2+2h+(1+h)^2]+2\left[\frac{\omega_p^2}{\omega_0^2}\right]\gamma_0^4(\beta_0^2+2h)^2-\gamma_0^6(1+\gamma_0^2h^2)(\beta_0^2+2h)^2\right\}$$
$$-\left[\frac{1}{2}\frac{(1+h)\omega_p^2/\omega_0^2}{\gamma_0^2(1+\gamma_0^2h^2)}\left[\frac{b_+-b_-}{b_++b_-}\right]\right]^2. \tag{7}$$

The first-order term (in τ/R) of (6) describes the negative mass effect[1] and dc field effects, while the second-order term includes the diocotron effect[14] and finite-thickness stabilization.[3] The derivation of (6) will be given elsewhere. Its validity may be tested as follows:

(a) If the beam is infinitesimally thin, and if we ignore the dc electric field by setting $h=0$, we then recover from (6) the well-known dispersion relationship $\omega_i^2\cong(l\tau/R)\omega_p^2\beta_0^2/(b_++b_-)$ for the negative mass instability for the Astron geometry.[8,3,4,10]

(b) A more stringent test on the validity of (6) is to consider the planar geometry limit. In this limit, we let $R\to\infty$, $l\to\infty$, $\omega_0\to 0$, but require that v_0, $k_y=l/R$, E_0, and τ remain finite. Then $h\to\infty$ from (5) and the first term of the right-hand side of (6) tends to zero, consistent with the notion that there is no negative mass instability in a planar geometry. Using only the last term of (6), we then obtain

$$\omega_i^2\simeq(k_y^2\tau^2/4\gamma_0^8h^2)\omega_p^4/\omega_0^2=(k_y^2\tau^2/4\gamma_0^4)\omega_p^4/\omega_c^2$$

which agrees with the well-known growth rate for the diocotron instability for a sheet beam.[14] In writing the last expression, we have used the self-consistent equilibrium condition $E_0+v_0\times B_0=0$ (for a planar sheet beam) in (5) and defined $\omega_c=|e|B_0/m_0\gamma_0$. This agreement with previously known results adds to our confidence in the dispersion relationship (6), especially with regard to the effects of dc self-fields. Recent work on the diocotron instability is reported by Tsang and Davidson.[15]

For a thin E layer with sufficiently high energy ($\gtrsim 1$ MeV), the last term of (6) may be ignored. The dispersion relationship may then be approximated by

$$\omega_i^2 \cong \left|\frac{1}{b_+ + b_-}\right| \omega_p^2 \left(\frac{l\tau}{R}\right) \frac{(\beta_0^2+2h)}{(1+\gamma_0^2 h^2)}. \tag{8}$$

Thus, the sufficient condition for stability is

$$h < -\beta_0^2/2 \tag{9}$$

for the usual case[13] $b_+ + b_- > 0$. This stability condition (9), together with the definition of h in (5), implies that a sufficiently strong, radially inward electric field may render the relativistic electron beam stable against the negative mass instability. This stabilization is independent of the beam velocity spread or betatron motion, and since its derivation has already taken into consideration the dc self-field effects, the criterion (9) is not restricted to a low-current beam.[16] In the event that the externally imposed electric field exceeds the self-fields, the stability condition (9) may be rewritten as

$$|e\phi| > \tfrac{511}{2}\beta_0^4\gamma_0^3 \ln(b/a), \tag{10}$$

where $|e\phi|$ is the externally imposed potential difference (in kiloelectronvolts) between $r=a$ (the cathode) and $r=b$ (the anode).

As an example, take $R=100$ cm, $b-a=4$ cm. Then, according to (10), a 1-MeV electron beam would be stable against the negative mass instability if the inner conductor is negatively biased at a voltage greater than 200 keV with respect to the outer conductor.

A partial explanation of the stability condition (9) may be given in terms of the single particle motion in an *externally* imposed field E_0 and B_0. Let ϵ be the total energy (kinetic and potential) of an electron. One may easily deduce from (1) that $d\omega_0/d\epsilon=(d\omega_0/dr)dr/d\epsilon \propto (\beta_0^2+2h)/(1+\gamma_0^2h^2)$ if the self-fields of the electron layer are neglected. Thus, the effective azimuthal inertia[1,9] of a rotating relativistic electron may be converted from negative to positive if h is less than $-\beta_0^2/2$. It should be stressed, however, that the stability condition (9) is derived from collective-mode considerations which include *both* the ac and the dc self-fields.[17]

In summary, this Letter presents a novel, robust method to suppress a major instability in circular accelerators. Technical aspects such as fabrication, beam injection, and beam retrieval remain to be studied. A more refined analysis may be needed to examine the possible occurrence (if any) of residual instabilities. The stability criterion (9) may be tested on several currently operating devices.

We would like to thank P. Sprangle, I. B. Bernstein, and L. R. Barnett for discussion, and B. H. Hui and J. M. Mangano for encouragement. This work is supported by the U. S. Office of Naval Research.

---

[a]Also at Berkeley Research Associates, Springfield, Va. 22150.

[1]C. E. Nielson, A. M. Sessler, and K. R. Symon, in *Proceedings of the International Conference on Accelerators* (CERN, Geneva, 1959), p. 239; also A. A. Kolomenskii and A. N. Lebedev, *ibid.* p. 115.

[2]R. W. Landau and V. K. Neil, Phys. Fluids **9**, 2412 (1966); also R. W. Landau, Phys. Fluids **11**, 208 (1968).

[3]Y. Y. Lau and R. J. Briggs, Phys. Fluids **14**, 967 (1971).

[4]H. S. Uhm and R. C. Davidson, Phys. Fluids **20**, 771 (1977), and **21**, 265 (1978).

[5]P. Sprangel and J. L. Vomvoridis, U. S. Naval Research Laboratory Memorandum Report No. 4688, 1981 (unpublished).

[6]P. Sprangle and D. Chernin, Part. Accel. (to be published).

[7]P. Sprangle and C. A. Kapetanakos, J. Appl. Phys. **49**, 1 (1978); also N. Rostoker, Comments Plasma Phys. **6**, 91 (1980).

[8]R. J. Briggs and V. K. Neil, Plasma Phys. **9**, 209 (1967), and J. Nucl. Phys., Pt. C **8**, 255 (1966).

[9]V. K. Neil and W. Heckrotte, J. Appl. Phys. **36**, 2761 (1965).

[10]See, e.g., Y. Y. Lau, J. M. Baird, L. R. Barnett, K. R. Chu, and V. L. Granatstein, Int. J. Electron. **51**, 331 (1981), also Y. Y. Lau, IEEE Trans. Electron Devices **29**, 320 (1982), and references therein.

[11]I. Alexeff and F. Dyer, Phys. Rev. Lett. **43**, 351 (1980). See also L. R. Barnett, doctoral dissertation, University of Tennessee, Knoxville, 1978 (unpublished), for a related device.

[12]See, e.g., O. Buneman, R. H. Levy, and L. M. Linson, J. Appl. Phys. **37**, 3203 (1966), and references therein.

[13]The expressions for b_+ and b_- for the present geometry are given by Eqs. (49) and (50) of Ref. 8, where it is shown that $1/[|\epsilon_0|(b_+ + b_-)]$ is equivalent to

the geometrical g factor for the toroidal configuration treated in Ref. 1. For the toroidal configuration, g is always positive.

[14]O. Buneman, J. Electron. Control 3, 507 (1957).

[15]K. Tsang and R. C. Davidson, Bull. Am. Phys. Soc. 28, 1211 (1983).

[16]If the container wall is lossy, the wave admittance $(b_+ + b_-)$ would be complex. The electron beam may then be subject to resistive wall instabilities even if the stability criterion (9) is satisfied. The resistive growth rate and the negative mass growth rate scale differently, however. We wish to thank A. M. Sessler (private communication) for reminding us of the importance of resistive wall instabilities, and for furnishing an argument supporting our conclusion on the stabilization mechanism.

[17]It is of some interest to note that the negative mass factor $d\omega_0/d\epsilon$ is maximized with respect to h when $h = 1/\gamma_0^2$. Thus, according to Eqs. (1) and (5), the E layer is most unstable, and is therefore most likely to yield radiation, if its equilibrium rotation is *solely* supported by a radially outward electric field. Reference 11 reported a potent radiation source of this type. Moreover, since the dispersion relationship (8) is applicable for arbitrary combinations of E_0 and B_0, and for arbitrary energy of the electron beam, it provides a ready comparison of the "potency" among various microwave devices such as the gyrotron, orbitron, heliotron, and cross-field devices (if the small-signal growth rate is used as a criterion). Further discussions, as well as the confirmation of the stability criterion (9) by a numerical integration of (4), will be reported elsewhere.

APPENDIX B

Stability of Laminar Electron Layers

D. Chernin and Y.Y. Lau

TABLE OF CONTENTS

I. Introduction

There exists by now a truly enormous literature on the subjects of the equilibrium and stability of layers of charged particles in various geometries. The earliest studies[1-7] were conducted in order to understand the "slipping stream" or diocotron effect in the operation of the first magnetrons. Somewhat later the importance of curvature effects was realized when beams became relativistic, as in particle accelerators; the resulting "negative mass" instability[8,9] completely dominates the planar beam diocotron effect at sufficiently high energies (only a few tens of keV in many practical devices of interest). The negative mass effect was also investigated in connection with some controlled fusion research devices[10-12] and other machines.[13]

In recent times there has been renewed interest in high power, high efficiency microwave devices as well as in accelerators capable of high current operation. Spurred by the discovery of the electron cyclotron maser (or gyrotron) effect,[14-16] research in the field of short wavelength, high power microwave devices requiring no slow wave structure has been vigorously pursued.[17] Operation of these new devices depends fundamentally on the negative mass effect as enhanced by a synchronism of the particles' angular motion with the temporal and angular variation of a "cold" waveguide mode. This enhancement, though not called the maser effect, was first noted in the classic work of Briggs and Neil[10] and has been further elaborated in ref. 18.

The acceleration of large currents of electrons is a formidable problem which has also received considerable attention recently. In cyclic devices it is possible to construct high current equilibria in many cases[19-21] but various instabilities, the negative mass instability prominent among them, may limit achievable currents to smaller values than equilibrium considerations

alone would suggest. In these devices the effects of self fields on the negative mass instability and on the stabilization mechanism become important to consider; in one device these effects have been predicted to lead to a peculiar double-valued feature in the current vs. energy spread stability curve.[22] It was this particular result which initially prompted the study of self field effects reported here for a simpler (2D) model.

The model we consider consists of a layer of charged particles (we will think of them as electrons but ions may be trivially substituted) moving in circles about a common axis, as shown in Fig. 1. This restriction to laminar or "cold" electron flow will tend to overestimate actual growth rates of the modes we study since the effects of betatron oscillations and of nonaxis-encircling particles are stabilizing. An analysis including these effects is properly done in phase space using the correct equilibrium distribution function; such an analysis is significantly more complex than that given here and may be carried out only in an approximate way. The laminar flow case includes all essential physics and has great simplicity, allowing an exact treatment of the linearized problem, to recommend it. The equilibrium, discussed in the following section, is supported by a combination of self and externally applied radial electric and axial magnetic fields. We impose no a priori restriction on the relative magnitudes of the three terms—centrifugal force, electric force, $\hat{\mathbf{v}} \times \hat{\mathbf{B}}$ force--in the equilibrium force balance. This configuration is thus a reasonable model for the Astron,[23] magnetron, gyrotron, orbitron,[24] peniotron[25] and heliotron[26] and includes correctly the crucial radial and azimuthal particle dynamics found in particle accelerators. This "E-layer" model has the virtue that the linear stability problem may be formulated exactly, for arbitrary particle energies, including all effects of self fields and all effects of relativity and

electromagnetism. It is perhaps a bit surprising that, despite the venerability of the topic, this exact formulation has not been carried out earlier.[27] The eigenvalue problem governing the stability of the E-layer is derived and analyzed in Section III, below.

The desirability of a completely general treatment encompassing many devices and a large parameter space is related to the ease with which various familiar results for special cases may be recovered in appropriate limits. A dispersion relation for the so-called longitudinal mode obtained analytically in the thin beam limit from the ordinary differential equation governing the RF field reproduces all standard special case dispersion relations (negative mass, electron cyclotron maser, diocotron) in a straightforward way; in doing so, a puzzle is resolved concerning the survival of a finite negative mass growth rate in the planar limit and a method suggests itself on how either to maximize or eliminate altogether the negative mass instability growth.[28] Extensive testing of the dispersion relationship against a numerical solution of the eigenvalue problem shows excellent agreement, as reported in Section III. The classical diocotron dispersion relation is discussed and recovered from our formalism in Section IV.

Our treatment of the transverse mode, which has been invoked in the theory of the peniotron device[25] is somewhat less comprehensive. This mode is unstable only when electron motion is synchronous with a cavity mode and so is of a more specialized nature than the negative mass or diocotron instabilities which arise from intrinsic properties of geometry and shear flow, not from interaction with external structures. Still, the utility of the transverse mode for microwave generation may not yet have been fully exploited. We comment on some features of this mode in Section V.

II. Cold E-Layer Equilibrium

We consider an idealized model of an electron layer in which all electrons circle a common axis as shown in Fig. 1. We will neglect the effects of betatron oscillations and of axial motion in both perturbed and unperturbed states. Inclusion of betatron oscillations or axial perturbations is expected to have a stabilizing influence on the collective modes we will study. We further assume that in general the layer is enclosed in a coaxial waveguide with smooth, perfectly conducting walls at r=a and r=b, as shown in the figure. Absence of either or both walls results only in a change of certain boundary conditions.

Though this model is simple to describe it is surprisingly rich in content. Depending on beam and geometric parameters and types of applied fields, it may be taken as a good description of the Astron,[23] gyrotron,[17] orbitron,[24] peniotron,[25] heliotron[26] and cross field microwave devices and may also be of some interest in accelerator[8,9] and space physics stability problems as well as in the theory of magnetic insulation.

The equations governing the equilibrium quantities $v_o(r)\hat{\theta}$, $E_o(r)\hat{r}$, $B_o(r)\hat{z}$ for a specified density profile $n_o(r)$ are

$$\frac{\gamma_o v_o^2}{r} = \frac{e}{m}\left[E_o + v_o B_o\right] \tag{1}$$

$$\frac{1}{r}\frac{d}{dr}\left(rE_o\right) = -en_o/\varepsilon_o \tag{2}$$

$$\frac{dB_o}{dr} = \mu_o e n_o v_o, \tag{3}$$

where $-e$ and m are the electron charge and mass, γ_o is the usual relativistic factor, $\left(1-(v_o/c)^2\right)^{-1/2}$, c is the speed of light in vacuum, and ε_o and μ_o are

the permittivity and permeability of free space. In addition to the density profile, we take as given the total electrostatic potential difference and the total magnetic flux contained between r=a and r=b.

Using these conditions the solution to Eq. (2) is immediate and Eqs. (1) and (3) may be combined to yield a single differential equation for $u \equiv \beta_o\gamma_o \equiv v_o\gamma_o/c$:

$$u' = \frac{u}{r}\left[\frac{1 - \xi/\gamma_o^2 - \gamma_o^2 h}{1 + h}\right] \tag{4}$$

where $\xi = \omega_p^2/\omega_o^2$, $\omega_p^2 = e^2 n_o/m\gamma_o\varepsilon_o$ is the plasma frequency of the layer, $\omega_o = v_o/r$, and a prime denotes d/dr. In Eq. (4) we introduce the important quantity h, defined by,

$$h = \frac{erE_o}{mc^2\beta_o^2\gamma_o^3} \tag{5}$$

which is $(1/\gamma_o^2)$ times the ratio of the electric force to the centrifugal force experienced by an electron in equilibrium at radius r.

Equation (4) must be solved subject to an initial condition $u(r_1)$ satisfying Eq. (1) which we rewrite in the dimensionless form

$$u^2 = \alpha_E(u^2+1)^{1/2} + \alpha_B u \tag{6}$$

where $\alpha_E = erE_o/mc^2$ and $\alpha_B = erB_o/mc$. α_E is known at r_1 but α_B is not. The entire equilibrium problem then reduces to choosing $\alpha_B(r_1)$ such that the resulting total flux

$$\phi_o = 2\pi\int_a^b dr\ rB_o \tag{7}$$

is a specified number. A numerical method for doing this is described in Appendix A. Here we briefly consider the character of some of the solutions. The equilibrium thus constructed will be used in the numerical solution of the eigenvalue problem in Section III.

Given $\alpha_E(r_1)$ and $\alpha_B(r_1)$, Eq. (6) may have 0, 1, or 2 real valued solutions for $u(r_1)$, depending on the values of α_E and α_B; without loss of generality we take $\alpha_B(r_1) > 0$. The situation in the $\alpha_E - \alpha_B$ plane is then depicted in Fig. 2. By a positive root, denoted by (+) in the figure, we mean a right-handed rotation about $\hat{B}$ (clockwise, looking in the direction of $\hat{B}$). The equation for the boundary curve C in Fig. 2 is the condition for Eq. (6) to have a double root:

$$\alpha_E = \frac{u^*(u^* - \alpha_B)}{(u^{*2} + 1)^{1/2}} \tag{8}$$

where $u^* = (8/3)^{1/2} \sinh\left[\frac{1}{3} \sinh^{-1}\left[\frac{1}{2}(3/2)^{3/2}\alpha_B\right]\right]$. On C, $1 + h = 0$.

There are three basic types of equilibria found in devices of practical interest: Type I, in which a magnetic field is used to balance centrifugal force (α_E is small, e.g. Astron, gyrotron, particle accelerators); Type II, in which electric and magnetic forces balance (inertia is small, e.g. crossed field microwave devices); and Type III, in which an electric field is used to balance centrifugal force (α_B is small, e.g. orbitron, heliotron). Type I may have only "+" roots while Types II and III may have either "+" or "-" roots. In the following analysis, however, we make no assumption regarding the relative magnitudes of the electric field, magnetic field, and inertia terms.

It is reasonable to ask whether stability considerations favor one type of equilibrium over another for a layer of given kinetic energy. To our knowledge there has been no definitive answer to this fundamental question.

For radiation source applications one arguably might want the most unstable configuration while for other applications, like accelerators, one would want the most stable one. We proceed to examine the stability of a general equilibrium describable by Eqs. (1) - (3) in order to address this question, our goal being a complete parametric study of the small signal behavior.

III. Stability of the Layer

We consider perturbations on the equilibrium described in the previous section. The equations governing the layer are, simply

$$(\frac{\partial}{\partial t} + \vec{v}\cdot\vec{\nabla})\gamma\vec{v} = -\frac{e}{m}(\vec{E} + \vec{v}\times\vec{B}) \qquad (9)$$

$$\vec{\nabla}\times\vec{E} = -\frac{\partial\vec{B}}{\partial t} \qquad \vec{\nabla}\cdot\vec{E} = -en/\varepsilon_o \qquad (10a,b)$$

$$\vec{\nabla}\times\vec{B} = \frac{1}{c^2}\frac{\partial\vec{E}}{\partial t} - \mu_o en\vec{v} \qquad \vec{\nabla}\cdot\vec{B} = 0 \qquad (11a,b)$$

where n is the number density.

Our discussion will be limited to consideration of perturbations in the $\hat{r}$ and $\hat{\theta}$ directions, for reasons described below. Writing all quantities Ψ as

$$\Psi(r,\theta,t) = \Psi_o(r) + \sum_{\ell}\int\frac{d\omega}{2\pi}\, e^{-i(\omega t-\ell\theta)}\Psi_1^{(\ell)}(r;\omega) \qquad (12)$$

where $\Psi_o(r)$ is the equilibrium value, and retaining only terms linear in $\Psi_1^{(\ell)}$ one finds that the linearized versions of Eqs. (9) - (11) decouple into two sets governing $\{v_{1r}, v_{1\theta}, E_{1r}, E_{1\theta}, B_{1z}, n_1\}$ and $\{v_{1z}, E_{1z}, B_{1r}, B_{1\theta}\}$ which we identify as TE modes and TM modes respectively. (Here and below we

write $\Psi_1^{(\ell)}(r;\omega)$ simply as Ψ_1 for all first order quantities.) The TM modes may easily be shown to be neutrally stable for perfect conductor boundary conditions (damped, for resistive wall boundary conditions). They represent simple oscillations of the electrons along the $\hat{z}$ direction in response to the cavity mode fields; the equilibrium model does not provide any free energy to excite the TM modes. The TE modes, on the other hand, are potentially unstable. If we had allowed a finite axial wavelength for the perturbed quantities the TM and TE modes would be coupled, but it has been found[10] that the effects of finite axial wavelength are stabilizing for the coupled case. Consequently we focus attention exclusively on the TE waves.

The Euler equation (9), upon linearization, gives the fluid response in terms of the RF fields of the TE wave:

$$-i\Omega v_{1r} - \omega_o P v_{1\theta} = -\frac{e}{m\gamma_o}[E_{1r} + v_o B_{1z}] \tag{13a}$$

$$\omega_o Q v_{1r} - i\Omega v_{1\theta} = -\frac{e}{m\gamma_o^3} E_{1\theta} \tag{13b}$$

where we have defined $\Omega = \omega - \ell\omega_o$, $P = \gamma_o^2(1+h)$, $Q = v_o'/\omega_o + h$, and $v_o' \equiv \frac{d}{dr} v_o$. Using the solution of Eqs. (13a,b) in the definitions of the RF currents J_{1r} and $J_{1\theta}$ and combining the linearized Maxwell's equations (10) - (11) allows one to write a single differential equation for $\phi \equiv rE_{1\theta}$:

$$r\frac{d}{dr}\left(r\tilde{A}\frac{d\phi}{dr}\right) + \tilde{C}\phi = 0 \tag{14}$$

where

$$\tilde{A} = \Delta^{-1}[1 + \xi/(D\gamma_o^2)] \tag{15}$$

$$\tilde{C} = \frac{\omega}{\Omega}\Big[\Big(\frac{\Omega}{\omega} - \frac{1}{\gamma_o^2}\Big)\frac{r}{\omega_o}\frac{\partial}{\partial r}\{\omega_o\Delta^{-1}D^{-1}\xi(1+h)\} + 2\beta_o^2\Delta^{-1}D^{-1}\xi(1+h)\Big]$$

$$+\Delta^{-1}D^{-1}(\xi/\gamma_o^2)\Big(\frac{\omega^2r^2}{c^2} - \ell^2 - \xi\beta_o^2\Big) + 1 \tag{16}$$

$$\Delta = \frac{\omega^2r^2}{c^2} - \ell^2 + D^{-1}\xi(\Omega^2r^2/c^2) \tag{17}$$

$$D = PQ - \Omega^2/\omega_o^2 = 1 - \xi/\gamma_o^2 + \gamma_o^2h^2 - \Omega^2/\omega_o^2 \tag{18}$$

and other symbols have been defined previously. [Equation (14) is identical to Eq. (4) of Ref. 28, except for a few differences in notation.]

The other RF fields are given in terms of ϕ by

$$E_{1r} = ir\Delta^{-1}\Big[\Big(\frac{\ell}{r} + \xi D^{-1}\Omega v_o/c^2\Big)\phi' - \frac{\omega\omega_o}{c^2}\xi D^{-1}(1+h)\phi\Big] \tag{19}$$

$$B_{1z} = -\frac{ir}{c^2}\Delta^{-1}\Big[(\omega + \xi D^{-1}\Omega)\phi' - \frac{\ell}{r}\omega_o\xi D^{-1}(1+h)\phi\Big] \tag{20}$$

and the perturbed velocities may be easily recovered using Eqs. (19) and (20) in Eqs. (13a,b); the perturbed density is obtained from $n_1 = -(\epsilon_o/e)\hat{\nabla}\cdot\hat{E}_1$.

Equation (14) must be solved subject to $\phi(a) = \phi(b) = 0$ (if the walls are perfect conductors) in order to obtain the eigenvalue, ω. Hereafter we shall assume that the electron layer is restricted to the annular region $r_1<r<r_2$ [Fig. 1]. In this case it is convenient to formulate the problem using the explicit vacuum solutions at $r=r_1$ and $r=r_2$ and to match the appropriate logarithmic derivatives, as is often done in microwave tube theory, in order to isolate the effect of wall boundary conditions. Defining, then, the

normalized admittances evaluated just outside of the layer, we have

$$b_+ \equiv -\left.\frac{iE_{1r}}{E_{1\theta}}\right|_{r=r_2^+} = \left.\frac{\ell r_2}{\frac{\omega^2 r_2^2}{c^2} - \ell^2}\,\frac{\phi'}{\phi}\right|_{r=r_2^+} \tag{21a}$$

$$b_- \equiv \left.\frac{iE_{1r}}{E_{1\theta}}\right|_{r=r_1^-} = \left.\frac{-\ell r_1}{\frac{\omega^2 r_1^2}{c^2} - \ell^2}\,\frac{\phi'}{\phi}\right|_{r=r_1^-}. \tag{21b}$$

We stress that the normalized wave admittances b_+ and b_- depend only on the waveguide geometry exterior to the electron beam. They are independent of the beam or its dynamics. b_+ and b_- are evaluated explicitly in Appendix B for some practical cases of interest.

Let us examine Eq. (14) more closely. In the complex r plane Eq. (14) has singularities at points where

$$\omega - \ell\omega_o = 0 \tag{22}$$

$$D + \xi/\gamma_o^2 = 0 \tag{23}$$

$$\Delta = 0. \tag{24}$$

The first of these clearly represents a match between the mode frequency and a harmonic of the particle "cyclotron" frequency. Such a match is present in the negative mass instability, cyclotron maser instability, and diocotron instability all of which are described by Eq. (14). Indeed, these may all be considered to be the same instability in this sense,[18] though the individual names are still useful. The negative mass instability is fundamentally a rotational effect. The classical explanation attributes it to the decrease of circulation frequency with particle energy leading to growth of azimuthal bunches. The negative mass instability operates without regard for the cavity

modes of the vacuum chamber; the fields are not well approximated by the cavity mode. The instability is strongly enhanced however if Re(ω) happens to be a cavity mode, as first pointed out by Briggs and Neil.[10] In recent years this synchronous case has been given its own name, the cyclotron maser instability, mainly in the literature of gyrotron research.[17,18]

The diocotron instability, originally studied in connection with the development of the first cross field microwave devices, is a "residual" instability in this context. It is what survives in the non-relativistic and/or planar limits. The perturbed electric fields are basically electrostatic in nature and are strongly localized at the position of the layer. The equation governing the diocotron instability[1,4,6,7,29] may be recovered formally from Eq. (14) by taking $c \to \infty$. It is discussed further in Section IV, below.

A mode satisfying Eq. (22) is sometimes called the longitudinal mode since the major effect on the beam is azimuthal bunching. Equation (23), on the other hand, describes what has been called the transverse mode which involves little bunching, but significant transverse (radial) motion of the beam. If h is small, Eq. (23) becomes

$$\omega - \ell\omega_o = \pm\, \omega_o . \qquad (25)$$

This transverse mode has been invoked to explain the operation of the peniotron[25] when ω corresponds to a cavity mode. In the nonsynchronous case the transverse mode is stable in the absence of resistive walls, as pointed out in ref. 10.

Finally we note that Eq. (24) may be loosely associated with an electromagnetic mode. In vacuum only (24) survives as a singularity but in

fact it may be shown to be only an "apparent" singularity;[30] the vacuum eigenfunctions are analytic in r, except possibly at r=0.

We proceed to analyze Eq. (14) to uncover the parametric dependences of the growth rates of the unstable modes. In order to make progress analytically we consider the case of a beam of uniform density and of thickness $\tau \equiv r_2 - r_1$ which is much less than its average radius $R \equiv \frac{1}{2}(r_2 + r_1)$. If the beam is sufficiently thin it is possible to consider a Taylor series solution about r=R of Eq. (14), taking care to check at the end that the singularities are sufficiently far away in the complex r plane, so as not to disturb the series convergence;[31] carrying out this program we find the dispersion relation

$$G_+ - G_- + \tau\left[\frac{C_o}{R^2 A_o} + \frac{1}{2}(G_+ + G_-)\left(\frac{A_1}{A_o} + \frac{1}{R}\right) + G_+ G_-\right]$$

$$- \frac{3}{8}\left(\frac{\tau}{R}\right)^2 (G_+ - G_-)\left(\frac{C_o}{A_o}\right) = 0 \qquad (26)$$

correct to order $(\tau/R)^2$. In Eq. (26) G_-, G_+ are the radial logarithmic derivatives of ϕ evaluated just <u>inside</u> the layer at $r=r_1$, $r=r_2$ respectively, obtained by integrating Eq. (14) across the beam edges:

$$G_\pm = \frac{-1}{r_{2,1}\tilde{A}(r_{2,1})}\left[\mp \frac{1}{\ell} b_\pm + q(r_{2,1})\right] \qquad (27)$$

where

$$q(r) = \frac{\omega}{\Omega}\left(\frac{\Omega}{\omega} - \frac{1}{\gamma_o^2}\right)\frac{\xi(1+h)}{\Delta D} \qquad (28)$$

and

$$\tilde{A}(r) \simeq A_o + (r-R)A_1 + \cdots \qquad (29)$$

$$\tilde{C}(r) \simeq C_o + \cdots$$

near r=R.

Expanding $G_\pm$ to order τ/R, Eq. (26) then reduces to

$$\frac{1}{\ell}(b_+ + b_-) + \frac{\tau}{R}\left[-Rq' - \frac{1}{A_o}\left(\frac{1}{\ell}b_+ - q\right)\left(\frac{1}{\ell}b_- + q\right) + C_o\right] = 0 \qquad (30)$$

where now q and q' are understood to be evaluated at r=R and where in Eq. (30) we have (temporarily) kept terms only to $O(\tau/R)$. No assumption has been made about the E-layer density or current; we have assumed only that the beam is "thin".

Let us first consider the longitudinal mode, that is, we look for a root of Eq. (30) with $|\Omega^2| << \omega_o^2$. Of the terms within the brackets in Eq. (30) only the q' and q^2 terms behave as Ω^{-2} for small Ω. Keeping only such terms, some algebra gives $\Omega_i \equiv \mathrm{Im}(\Omega)$:

$$\Omega_i^2 \equiv \frac{\ell \frac{\tau}{R}\omega_p^2}{(b_+ + b_-)} \frac{(\beta_o^2 + 2h)}{(1 + \gamma_o^2 h^2)} + O(\ell\tau/R)^2 \qquad (31)$$

which, for h = 0, is the classical negative mass dispersion relation for the Astron configuration.[10] (The $O(\ell\tau/R)^2$ term is displayed fully in Eq. (36), below.) We remark that Eq. (31), including the second order terms, can be obtained from the much simplified form of Eq. (26),

$$G_+ - G_- + \tau G_+ G_- = 0 \qquad (26')$$

where terms behaving as Ω^{-1} have been dropped from Eq. (26).

Ignoring the $O(\ell\tau/R)^2$ term in Eq. (31) for a moment, we may interpret the dispersion relationship (31) as follows. As we have seen, the factor $(b_+ + b_-)$ represents the effects of the container structure, and the factor $(\tau/R)\omega_p^2$ is proportional to the beam current. These two terms always appear in any dispersion relation involving an electron beam. All dynamical effects, including those due to self fields, are contained in the factor

$$M \equiv - \frac{(\beta_o^2 + 2h)}{(1 + \gamma_o^2 h^2)} \tag{32}$$

for a sufficiently thin beam. Some insight into the meaning of this factor may be had if we note that for small equilibrium densities, ξ, it is proportional to $d\omega_o/d\varepsilon$ where $\varepsilon = mc^2\gamma_o - e\phi_o$ is the total energy of a particle in the equilibrium:

$$\frac{d\omega_o}{d\varepsilon} = \frac{-\omega_o}{mc^2\gamma_o\beta_o^2}\left[\frac{\beta_o^2 + 2h + \xi/\gamma_o^4}{1 + \gamma_o^2 h^2 - \xi/\gamma_o^2}\right]. \tag{33}$$

At least when ξ is small then we find agreement with the classical explanation of the negative mass effect: A rotating beam is unstable (stable) if its equilibrium rotation frequency is a decreasing (increasing) function of its (total) energy, that is, M is proportional to the effective azimuthal inertia (mass). We stress that for finite ξ this interpretation begins to break down; Eq. (31) was derived assuming ξ was finite yet ξ does <u>not</u> appear in the factor M but clearly does appear in Eq. (33).

M, though simple in form, has many interesting features. Let us consider its dependence on h, illustrated in Fig. 3. Perhaps the most interesting property of M is that it experiences a change in sign at $h = -\beta_o^2/2$. The possibility for using this property of equilibria supported by a radially

inward electric field in addition to a magnetic field in order to suppress the negative mass instability has been discussed elsewhere.[28] We note that since the factor M is independent of the beam current or of the waveguide dimensions and represents a purely dynamical quantity, this stabilization of the negative mass instability by a radial electric field is expected to be valid even in toroidal geometry, even for high current, very cold beams. (The method is limited to use for moderately low energy beams, in the MeV range in practice, since the applied electric field required to change the sign of M from negative to positive is proportional to γ_o^3, as follows from the definition of h, Eq. (5).) Note that there is a "most stable" configuration at h=-1, at which point certain singular parts of $\tilde{C}$ in Eq. (14) vanish identically.

Perhaps equally interesting for microwave generation applications, is the occurrence of a "most unstable" point in Fig. 3 at $h = 1/\gamma_o^2$. If we recall that $\gamma_o^2 h$ is the ratio of the radial electric force to the centrifugal force we observe that the choice $\gamma_o^2 h = 1$ describes a configuration in which the equilibrium is supported solely by an electric field (a Type III equilibrium, in the language of Section II). This result suggests that for a given beam energy, a microwave source such as the orbitron[24] in which an annular beam circles a positively charged wire with no applied magnetic field, might have some advantage over more conventional devices like magnetrons (h<0), inverted magnetrons ($h>>1/\gamma_o^2$), or gyrotrons(h≈0). This finding is novel. We remark that this negative peak in M is sharpest at low energies (small β_o^2).

In the non-relativistic limit, $\beta_o^2 \to 0$, $\gamma_o^2 \to 1$, the sign of M is determined directly by the sign of h, which remains finite in this limit. Usually we are accustomed to thinking that the negative mass instability should vanish in the non-relativistic limit when there is no gradient in the magnetic field. Here we see however that an equilibrium electric field can affect the sign of

the azimuthal inertia just as a gradient in B can. If we define an equivalent field index, n_{eq}, by

$$\frac{1}{1- n_{eq}} - \frac{1}{\gamma_o^2} \equiv - M \tag{34}$$

then

$$n_{eq} = h\left[\frac{2 - (\gamma_o^2-1)h}{(1 + h)^2}\right] \tag{35}$$

which vanishes when h does.

One final comment about h must be made. The electric field appearing in the definition of h, Eq. (5), is due both to the electric charge of the layer and to any externally applied bias potential. When the contribution of the electric charge dominates there is some question as to what value of h to use in Eq. (31) when calculating growth rates since E_o and therefore h will change sign somewhere within the layer. For this reason, in all numerical examples considered below we will assume that h, when it is non-negligible, is dominated by the contribution of an externally maintained bias potential.

The analytical results presented up to this point are subject to test by numerical integration of Eq. (14) subject to suitable boundary conditions. We have written a program to carry out this task. Given a density profile, the electrostatic potential difference and the total magnetic flux contained between r=a and b, the program calculates all equilibrium quantities then, given the mode number ℓ, locates an eigenvalue ω. In all examples below the density profile is parabolic; we expect good agreement with Eq. (31), derived using a flat profile, if we identify $(\tau/R)\ \omega_p^2$ with $2(\nu/\gamma_o)(c^2/R^2)$ where ν is Budker's parameter, the number of particles per unit length times the

classical electron radius. All examples use a perfectly conducting wall; effects of a small wall resistivity, which may be very important under some conditions, are discussed briefly toward the end of Appendix B.

Though we shall eventually test Eq. (31) for all parameter dependences, let us first check the interesting dependence on h, discussed above, against a numerical solution of Eq. (14). Figure 4 presents some typical results. Here we have illustrated, for two different values of ν/γ_o a comparison of the $\ell = 1$ mode growth rates for a thin ($\tau/R = .02$) beam as predicted by Eq. (31) (dashed line) and by a solution of Eq. (14) (solid line). (To be precise, what is plotted on the numerical solution curve is $\mathrm{Im}(\omega)/\omega_o(r_1)$.) The transition from stable to unstable behavior occurs at $h = -\beta_o^2/2$ ($\simeq -0.278$ for this case) <u>independent</u> of ξ. This is an important feature of Eqs. (31) and (32) which has been used to argue[28] that the stabilization condition, $h<-\beta_o^2/2$, for the negative mass instability is independent of the beam current. Note that this statement cannot be made on the basis of single particle orbit theory alone [cf. Eq. (33)]; the stabilization condition is obtained from collective mode considerations including self field effects. Actually a small amount of residual growth remains for h less than but very close to $-\beta_o^2/2$, a feature discussed in more detail in the following section. Agreement between Eq. (31) and the numerical solution is best at small growth rates which is reasonable if we recall that terms behaving as Ω^{-1} were neglected in favor of terms behaving as Ω^{-2} when Eq. (31) was derived. Equation (31) consistently gives slightly too high a growth rate (i.e. it is pessimistic), a feature which will be shown to persist when variations of other parameters are considered. Notice that the numerical solution confirms the existence of a peak in the growth rate for $h = 1/\gamma_o^2$, as predicted by Eq. (31), again independent of ξ.

The significant parameters upon which the small signal behavior of the layer depends include, beside the externally applied bias fields, the geometry factors a, b, r_1, r_2, the current (ν), the beam energy γ_o, and the mode number ℓ. We proceed to consider the effect of each of these separately on the growth rate of the longitudinal mode, $\omega \approx \ell\omega_o$, for the specific case of an Astron-like configuration, $h \approx 0$.

Unless otherwise stated all parameters in the cases considered below will take the following nominal "base case" values: $a = 0.5$m, $b = 2.2$m, $r_1 = 0.99$m, $r_2 = 1.01$m, total electrostatic potential difference between inner and outer walls = 0., total flux between inner and outer walls = $\pi(b^2 - a^2)\, B_{oo}$ where $B_{oo} = 48.2\times10^{-4}$T is the field required to hold a single particle at R = 1m with $\gamma = 3$. The radial density profile is always taken to be parabolic and symmetric about r=R=1m with specified peak value; the base case value is 5×10^7/cc which gives $\nu/\gamma_o = 3.94\times10^{-3}$. The base case azimuthal mode number ℓ is 1, for which $b_+ + b_- \tilde{=} 2.50$ for $\omega = \omega_o$. From Eq. (31) the normalized growth rate for the base case is 5.6%; the numerical solution of the eigenvalue problem gives 5.35%.

Figure 5 illustrates the comparison of growth rates as calculated by Eq. (31) and by a numerical solution of the eigenvalue problem for a range of currents. Over the wide range considered, the $\nu^{1/2}$ scaling predicted by Eq. (31) is shown to hold up extremely well up to values of ν/γ_o of a few percent. Similar excellent agreement is generally found for variations in layer thickness (Fig. 6), outer wall position (Fig. 7), inner wall position (Fig. 8), particle energy (Fig. 9), and azimuthal mode number (Fig. 10). Some remarks on each case follow.

In the case of varying layer thickness with the maximum density fixed (Fig. 6) two effects are competing; these are the basic $\nu^{1/2}$ dependence of the

growth rate versus the stabilizing effect of finite thickness[30] (effectively, finite frequency spread). The finite thickness effect is clearly second order in (τ/R) and is not shown explicitly in Eq. (31) but it is included in all plotted data of Figs. 5 - 10; the second order term is given explicitly in the following section. In the examples we have studied, finite thickness effects have been small and have not been effective in stabilizing the instability.

In Fig. 7 the effect of outer wall position is illustrated. As the wall is moved in from its base case location at 2.2m the growth rate is observed to increase dramatically for a while, then to fall off. The reason for the increase is the approach to synchronism of particle motion with a cavity vacuum mode, that is, $\omega \approx \ell\omega_o \approx \omega_v$ where ω_v is a solution to $b_+ + b_- = 0$; under this synchronous condition the cavity mode fields act to enhance those established by the dynamical charge bunching due to the negative mass effect. This synchronous case has been given its own name, the cyclotron maser instability, and is put to enormous practical use in the gyrotron family of microwave devices.[17] While in Figs. 5 - 10 we have consistently evaluated b_+ and b_- at $\omega = \ell\omega_o$, near a zero of $b_+ + b_-$ this is clearly inadequate and Eq. (31) should be solved as a cubic polynomial. Empirically we find that evaluating $b_+ + b_-$ at $\omega = \ell\omega_o$ is adequate when $b_+ + b_- > \ell$.

As the outer wall is moved further inward, past the synchronous point the growth rate in Fig. 7 drops as $b_+ + b_-$ changes sign. This drop is attributable to a "shorting out" of the azimuthal field $E_{1\theta}$ as the wall approaches the edge of the layer. An identical phenomenon is seen as the inner wall is moved outward, Fig. 8. Use of an inductive impedance ($b_+ + b_- < 0$) to stabilize the negative mass instability has been proposed by Briggs and Neil.[32] We remark that in Fig. 8 no synchronous case is encountered for the parameters considered, as the inner wall is moved.

The decrease of growth rate with increasing kinetic energy is documented in Fig. 9. The basic reason for this decrease is just the relativistic mass increase: the azimuthal response of a particle to the perturbed field $E_{1\theta}$ is reduced by a factor γ_o^{-1}, for large γ_o. No synchronous cases are encountered over the range of γ_o considered.

In Fig. 10 we have plotted growth rate versus azimuthal mode number ℓ. Agreement is good between the dispersion relation, Eq. (31), and the numerical solution; near synchronous cases occur for $\ell = 5$ and 9. Though predicted growth rates are rather large, for the high ℓ modes, these should in practice be subject to stabilization by the effects of finite betatron oscillations which we have neglected in this treatment. In any event we expect the dispersion relation, Eq. (31), to begin to break down for short wavelengths, i.e. $\ell\tau/R \gtrsim O(1)$, or azimuthal wavelengths on the order of the layer thickness. A WKB treatment of Eq. (14) carried out for this case yields an eigenvalue condition, the numerical solution to which would appear to require more effort than a direct numerical solution of Eq. (14) itself.

Finally, we report that in the initial phase of our investigation, we attempted to derive the dispersion relationship by constructing a quadratic form for the differential equation (14), under the assumption that $\phi = rE_{1\theta}$ is approximately constant across the E-layer. The latter assumption has been widely used and has been considered valid[9-11,17,18] for a thin relativistic electron beam. However, this line of investigation led to an incorrect dispersion relationship if $\omega_p^2/\omega_o^2 \gtrsim O(1)$, even to the lowest order in τ/R. In other words, to account correctly for the DC self fields in the present Eulerian description, the tangential AC electric field should not be assumed constant across the E-layer, regardless of the thickness. On the other hand, our dispersion relationship Eq. (31) correctly accounts for the self fields,

and is valid for arbitrary beam energy, and arbitrary combination of E_o and B_o, as already stressed.

IV. Residual Growth: The Diocotron Instability

Sufficiently close to the "zero mass" points $h = -\beta_o^2/2$, $h \to \pm\infty$, Eq. (31) begins to be dominated by the neglected terms of order $(\tau/R)^2$. We have already observed this phenomenon near the point $h = -\beta_o^2/2$ in Fig 4. In this section we discuss the point $h \to \pm\infty$, which extreme is reached in the planar limit: $r \to \infty$, $\ell \to \infty$, $\ell/r \equiv k_y$ finite. We remark that the vanishing of the negative mass growth rate in the planar limit, a feature of Eq. (31) and clearly expected on physical grounds, has not previously been demonstrated analytically, to the authors' knowledge.

The second order term in Eq. (31) is given, in complete generality, by $(\ell\tau/R)^2\omega_o^2\Lambda$ where

$$\Lambda = \frac{1}{4\gamma_o^6(1+h)^2(1+\gamma_o^2h^2)}\left[\xi^2\left(\beta_o^2 + 2h + (1+h)^2\right)\right.$$

$$\left. +2\xi\gamma_o^4\left(\beta_o^2 + 2h\right)^2 - \gamma_o^6(1+\gamma_o^2h^2)\left(\beta_o^2 + 2h\right)^2\right]$$

$$- \left[\frac{\xi}{2}\,\frac{(1+h)}{\gamma_o^2(1+\gamma_o^2h^2)}\left(\frac{b_+ - b_-}{b_+ + b_-}\right)\right]^2. \qquad (36)$$

As it stands Λ includes both the diocotron instability (ξ^2 terms) and the finite thickness stabilization effect[30] (ξ^0 term) referred to above. The last term of Eq. (36) contains wall boundary effects; specifically we may recover the stabilization at the diocotron mode due to contact of the layer with perfectly conducting walls,[6] as well as the destabilizing effects of finite wall conductivity.[34-37] If we assume that the walls are many wavelengths away

and that the fields are electrostatic then, in the planar limit, $b_{\pm} = 1$. Taking, then, the planar limit, $h\omega_{o+} - eB_o/(m\gamma_o^3) \equiv -\omega_c/\gamma_o^2$, only the first ξ^2 term in Eq. (36) survives and we recover the classical result[4] for the growth rate of the diocotron mode

$$\mathrm{Im}(\omega) = |k_{y\tau} v_o'/2| \tag{37}$$

where the velocity shear $v_o' = \omega_p^2/(\omega_c \gamma_o^2)$. Of course Eq. (37) may be obtained by much simpler methods than those employed here; our point is only that it is recoverable from the present formalism. Note that the dependence on the line density, ν, of the diocotron growth rate is just ν^1; for the (non-synchronous) negative mass instability the dependence is $\nu^{1/2}$; for the synchronous case it is $\nu^{1/3}$.

The relationship between the diocotron and negative mass instabilities has been discussed by Neil and Heckrotte[38] and by Lau.[18] Mostrom and Jones[39] have recently examined the electrostatic case, including the effects of shear in v_z. Davidson and Tsang[29] have reported analytical and numerical results in cylindrical geometry.

V. The Transverse Mode

An electron moving in a field satisfying Eq. (25) where $\mathrm{Re}(\omega)$ is a vacuum guide mode may be shown to be acted upon by a nearly constant electric field, when the motion is averaged over its gyro-orbit. The particle therefore experiences an $\hat{E} \times \hat{B}$ drift transversely, toward the wall, which motion brings the particle to experience yet a stronger electric field. A net transfer of energy from (to) the particles may be shown to result for the - (+) sign resonance of Eq. (25). This mechanism of wave growth has been used to explain

the operation of the peniotron oscillator.[25]

In the planar limit of the previous section, the resonance condition for the transverse mode, Eq. (23), becomes $\gamma_o(\omega - k_y v_o) = \pm \omega_c$, which is the well-studied mode of planar magnetron tube theory.[1-7,33,34] The factor h, [Eq. (5)], thus again appears, as it did in Eq. (31), as a measure of the "planarity" of the configuration.

A dispersion relation for the transverse mode may also be obtained from Eq. (30). Keeping the most important terms we have, approximately

$$\frac{1}{\ell}(b_+ + b_-) - \frac{\tau}{R}\frac{1}{A_o}\left(\frac{1}{\ell}b_+ - q\right)\left(\frac{1}{\ell}b_- + q\right) = 0 \qquad (38)$$

where, near the zeroes of A_o

$$A_o \simeq \frac{-(\Omega^2 - \alpha^2\omega_o^2)}{\ell^2\omega_p^2\left(1 - \beta_o^2\frac{\omega}{\ell\omega_o}\right)^2} \qquad (39)$$

$$q \simeq \frac{-\omega_o}{\ell\Omega}\frac{(1+h)}{\left(1 - \beta_o^2\frac{\omega}{\ell\omega_o}\right)} \qquad (40)$$

where $\alpha^2 = 1 + \gamma_o^2 h^2$. Equation (38), using Eqs. (39) and (40), agrees with Eq. (39) of Briggs and Neil[10] for $h = 0$, to leading order in ξ.

Clearly there are no unstable roots of Eq. (38) near the (simple) zeroes of A_o unless either one of these nearly coincides with a zero of $b_+ + b_-$ (a guide mode cutoff frequency) or b_+ or b_- contains an imaginary part, due to finite wall resistivity for example (see Appendix B). Thus the transverse mode (for small h) depends crucially on the interaction of the electrons with their external surroundings, unlike the negative mass and diocotron instabilities, the mechanisms of which operate in a manner that is insensitive to boundary conditions on the fields at distant walls. In the synchronous

case, with perfectly conducting walls the predicted scaling of the growth rate of the transverse mode with ν is $\nu^{1/2}$. The dependence of the real part of the frequency of the mode on an externally applied radial DC electric field may prove useful in some circumstances.

The peniotron interaction is essentially non-relativistic. It relies heavily on the spatial inhomogeneity of the perturbed wave fields. In contrast, for longitudinal modes, the spatial inhomogeneity of the unperturbed motion (i.e. shear) is far more important. Both the transverse and longitudinal modes can be used to convert the rotational energy of the electrons to rf waves efficiently, however.

In the planar limit Eq. (38) continues to predict stability in the absence of a resistive wall yet it is well-known[1-5] that inclusion of a resonant layer satisfying $\gamma_o(\omega - k_y v_o) = \pm \omega_c$ in the beam leads to wave growth. The resolution of this contradiction lies in the failure of the Taylor series solution to Eq. (14), from which Eq. (38) was obtained; the resulting growth rate is non-analytic in ξ and one must resort to numerical or other methods[7] to solve the eigenvalue problem.

VI. Summary

In this paper we have attempted a general treatment of the linear stability problem for laminar electron flow in cylindrical geometry. The basic equilibrium state has been taken to be maintained by radial electric and/or axial magnetic fields (Eq. (1)). No azimuthal magnetic field nor any axial electron motion have been included in the equilibrium state. The linear stability problem for azimuthal and radial perturbations has been formulated exactly, fully relativistically and fully electromagnetically, including all effects of self fields. The stability problem reduces to an eigenvalue problem for the frequency ω, given the azimuthal mode number, ℓ (Eq. (14), with associated boundary conditions).

Our efforts have been focused on the longitudinal mode (Eq. (22)), for thin beams, which is of considerable importance in accelerator and microwave device research. We have obtained, and favorably compared to a numerical solution of the eigenvalue problem, a dispersion relation in the thin beam limit (Eq. (31)) which applies in complete generality to the longitudinal mode and which reproduces all classical results in appropriate limits. Some interesting differences among equilibria regarding the negative mass instability have been pointed out; namely we have found a simple way either to stabilize or to maximize the growth of this mode. This finding might have practical consequences in accelerator or microwave tube design.

The longitudinal mode, $\omega - \ell\omega_o \approx 0$, encompasses the negative mass, electron cyclotron maser, and diocotron instabilities. The negative mass and electron cyclotron maser effects are unique to cylindrical geometry; they are fundamentally relativistic in nature when the motion is supported solely by a magnetic field. They are even more pronounced, especially for low energy beams, if the equilibrium rotation is supported solely by a radial electric

field. In planar geometry both of these instabilities are absent and only the residual diocotron instability remains which itself may be stabilized by placing the layer in contact with a conducting wall.[6]

The transverse mode, $\omega - \ell\omega_o = \pm \alpha\omega_o$ (α is defined following Eq. (40)) has been used to explain the operation of the peniotron device. When the geometry is cylindrical ($|\gamma_o h| \ll 1$) this mode is stable unless the electron motion is synchronous with a cavity mode and/or resistive walls are present. In the planar limit $\alpha\omega_o \to \omega_c/\gamma_o$ and we identify this mode as the Doppler shifted cyclotron resonance considered by Buneman[4,5] and others[1,6,7,33] in studies of magnetron operation. This mode is the dominant unstable mode for planar, high density laminar flow.

Finally we remark that the singularities defined by Eq. (24), which we have not examined here, may be worth some additional study; however we note that in both the vacuum case,[30] $\xi = 0$, and in the case of planar Brillouin flow,[1,2,5,33] $\omega_p^2 = \omega_c^2$, the singularity, Eq. (24), is removable.

VII. Acknowledgments

We wish to thank I. Bernstein and P. Sprangle for several helpful discussions and A. M. Sessler for correspondence.

This work was supported by the Office of Naval Research.

Appendix A

Technique for Numerical Solution of Equilibrium Problem

In this Appendix we describe a simple technique based on Newton's method which we have used to solve a certain eigenvalue problem associated with the calculation of laminar E-layer equilibria. Given the electric field which is trivially solved for, having specified the density profile and potential on one wall, we must find the momentum profile, u(r) and the field $B_o(r)$ subject to the constraint of specified total flux Eq. (7). The total flux might be specified in an experiment in which a beam is injected and contained in a chamber for less than a magnetic diffusion time.

Let us cast the problem in terms of the dimensionless fields, α_E and α_B defined in the text following Eq. (6). The problem then is to find u(r) and $\alpha_B(r)$ subject to

$$\int_a^b dr\ \alpha_B \equiv F \equiv \text{specified constant} \qquad \text{(A-1)}$$

where u and α_B satisfy

$$u' = \frac{u}{r}\left[\frac{1-\xi/\gamma_o^2 - \gamma_o^2 h}{1+h}\right] \qquad \text{(A-2)}$$

$$\left(\frac{1}{r}\alpha_B\right)' = \frac{\omega_p^2}{c^2}u \qquad \text{(A-3)}$$

$$u^2 = \alpha_E(u^2+1)^{1/2} + \alpha_B u \qquad \text{(A-4)}$$

for $r_1 < r < r_2$. Equation (A-2) guarantees that if $u(r_1)$ satisfies Eq. (A-4) then u(r) will do so for all r. The algorithm proceeds as follows: An initial guess is made for $\alpha_B(r_1)$ using the value of the externally applied B field,

say. Using the known value of $\alpha_E(r_1)$ the roots (two, in general) of Eq. (A-4) are found and the one corresponding to the equilibrium of interest is chosen. Equations (A-2) and (A-3) are then integrated and the difference

$$\int_a^b dr\ \alpha_B - F \equiv D^* \qquad \text{(A-5)}$$

is calculated. $\alpha_B(r_1)$ is then adjusted according to

$$\alpha_{B,n+1} = \alpha_{B,n} - \frac{D^*}{\int_a^b dr \frac{\partial \alpha_{B,n}(r)}{\partial \alpha_{B,n}(r_1)}} \qquad \text{(A-6)}$$

where the subscript n denotes an iteration number. The loop is stopped once D* is less than some specified tolerance.

It remains only to describe the evaluation of the denominator in Eq. (A-6): The dependence of $\alpha_B(r)$ on its initial condition at r_1 is found during the integration of Eqs. (A-2) and (A-3) by simultaneously integrating the equations for $\partial\alpha_B(r)/\partial\alpha_B(r_1)$ and $\partial u(r)/\partial\alpha_B(r_1)$ which are simply obtained by explicitly differentiating Eqs. (A-2) and (A-3) with respect to $\alpha_B(r_1)$. The initial condition $\partial u(r_1)/\partial\alpha_B(r_1)$ is obtained from Eq. (A-4).

Appendix B

Evaluation of the TE Wave Admittances

In this Appendix the normalized admittances $b_\pm$ referred to in the text in Eqs. (21a,b) are given for the geometry of Fig. 1; the toroidal and planar cases are also discussed.

In the vacuum regions $a<r<r_1$ and $r_2<r<b$ the wave equation Eq. (14) is

$$r\frac{d}{dr}\left(\frac{r}{\frac{\omega^2 r^2}{c^2} - \ell^2}\frac{d\phi}{dr}\right) + \phi = 0 \qquad \text{(B-1)}$$

the general solution to which is

$$\phi = x\left[C_1 J_\ell'(x) + C_2 Y_\ell'(x)\right] \qquad \text{(B-2)}$$

where $x = \omega r/c$, J_ℓ and Y_ℓ are the standard Bessel functions, C_1 and C_2 are constants, and in this Appendix a prime will denote $\frac{d}{dx}$. Note that the "singularities" at $x^2 = \ell^2$ in Eq. (B-1) are only apparent, not real, i.e. ϕ is analytic at these points. The other vacuum fields are

$$E_{1r} = \frac{i\ell}{x^2 - \ell^2}\frac{d\phi}{dr}, \qquad \text{(B-3)}$$

$$B_{1z} = -\frac{x}{c\ell}E_{1r}. \qquad \text{(B-4)}$$

Using the definitions in the text Eqs. (21a,b), it follows that $b_\pm$ may be generally written

$$b_+ = -\frac{\ell}{x_2}\left[\frac{C_1^+ J_\ell(x_2) + C_2^+ Y_\ell(x_2)}{C_1^+ J_\ell'(x_2) + C_2^+ Y_\ell'(x_2)}\right] \qquad \text{(B-5a)}$$

$$b_- = \frac{\ell}{x_1}\left[\frac{C_1^- J_\ell(x_1) + C_2^- Y_\ell(x_1)}{C_1^- J'_\ell(x_1) + C_2^- Y'_\ell(x_1)}\right] \qquad \text{(B-5b)}$$

where $x_{1,2} \equiv \omega r_{1,2}/c$.

The ratios C_1^+/C_2^+ and C_1^-/C_2^- are determined by the boundary conditions at r=b and r=a respectively. Some special cases of interest are:

1. Perfectly conducting wall at $r=r_w$: (r_w= a or b)

$$C_1/C_2 = -Y'_\ell(x_w)/J'_\ell(x_w) \qquad \text{(B-6)}$$

2. Wall with (complex) dielectric $\varepsilon(\omega)$:

$$C_1/C_2 = -\left[\frac{Y'_\ell(x_w) - (\zeta/\zeta_o)Y_\ell(x_w)\frac{d}{dy}\ln Z(y)}{J'_\ell(x_w) - (\zeta/\zeta_o)J_\ell(x_w)\frac{d}{dy}\ln Z(y)}\right] \qquad \text{(B-7)}$$

where ζ is the surface impedance, $(\mu/\varepsilon)^{1/2}$, $\zeta_o = 376.7\Omega$, $y = \kappa r_w$, $\kappa = \omega(\varepsilon\mu)^{1/2}$, $Z(y) = J_\ell(y)$ for inner wall, $H_\ell^{(1)}(y)$ for outer wall where $H_\ell^{(1)}$ is the Hankel function. ε and μ refer to the wall material.

3. No inner wall:

$$C_2^- = 0 \qquad \text{(B-8)}$$

4. No outer wall:

$$C_1^+/C_2^+ = -i \qquad \text{(B-9)}$$

5. Electrostatic limit; perfectly conducting walls at r=a,b:

$$b_+ = \frac{B_+ + 1}{B_+ - 1} \; ; \qquad b_- = \frac{B_- + 1}{B_- - 1} \tag{B-10}$$

where $B_+ \equiv (b/r_2)^{2\ell}$ and $B_- \equiv (r_1/a)^{2\ell}$. Note that $b_\pm > 0$.

6. Planar limit ($r \to \infty$, $\ell \to \infty$; $\ell/r \equiv k_y$, $b-a$, $b-r_1$, $b-r_2$, r_2-r_1, all remain finite); perfectly conducting walls:

$$b_+ = -(k_y/\alpha) \cot [\alpha(r_1-a)] \tag{B-11}$$

$$b_- = -(k_y/\alpha) \cot [\alpha(b-r_2)] \tag{B-12}$$

where $\alpha \equiv (\omega^2/c^2 - k_y^2)^{1/2}$. The planar limit of (B-10) is just the electrostatic limit of (B-11) and (B-12), as expected, in which case

$$b_+ = \coth [k_y(b-r_2)] \tag{B-13}$$

$$b_- = \coth [k_y(r_1-a)]. \tag{B-14}$$

When a wall is resistive the resulting dissipation is represented by an imaginary part in the corresponding admittance $b_\pm$. (In Eq. (B-7) $\epsilon(\omega) = i\sigma/\omega$ for a good conductor of conductivity σ.) That such dissipation can lead to disruptive beam instabilities, even for a "positive mass" beam, has been known since the pioneering work of Neil and Sessler[35] and Laslett, Neil, and Sessler.[36] It is in fact these resistive modes, rather than the (fundamentally dynamical) negative mass instability which are thought

ultimately to limit the beam current in cyclic electron accelerators.

If a wall is not smooth but contains some structures (cavities, fins, etc.) a common practice is to calculate an approximate value for the admittance and to use it as a boundary condition for some approximation to Eq. (14) in the text. In this case however the problem is not being treated fully self consistently since the equilibrium of Section II would not be strictly correct, i.e., the correct equilibrium would no longer have azimuthal symmetry (and would be much harder to calculate).

For the case of a perfectly conducting wall we have plotted in Figs. B-1,2,3,4 the quantity $b_+ + b_-$ evaluated for $x_1 \tilde{=} x_2 \tilde{=} \ell\beta_o$ for various values of $E_\perp \equiv mc^2(\gamma_o - 1)$, assuming a thin layer. It is this quantity, $b_+ + b_-$, which enters the dispersion relation for the longitudinal mode discussed in the text.

For a toroidal (accelerator) geometry, the dispersion relation Eq. (31) is expected to be replaced by

$$\Omega_i^2 = -\varepsilon_o g \ell^2 (2\nu/\gamma_o)(c^2/R^2)(mc^2/\omega_o)(\partial\omega_o/\partial\varepsilon)_{ext} \qquad \text{(B-15)}$$

where $(\partial\omega_o/\partial\varepsilon)_{ext}$ denotes the derivative of the circulation frequency with respect to total particle energy evaluated as if the particle were acted upon only by the external electric and magnetic fields. In Eq. (B-15), we have identified the geometric factor g of refs. [8,11] with $1/(\ell\varepsilon_o(b_+ + b_-))$, as pointed out in ref. 10. Note that the dispersion relationship (B-15) includes self field effects and that g is always positive for toroidal geometry (with smooth, perfectly conducting walls).

References

1. G. C. MacFarlane and H. G. Hay, Proc. Phys. Soc. (London) B63, 409 (1950).
2. O. Buneman, in Proc. Conf. Dynamics of Ionized Media, R.L.F. Boyd, ed. (University College, London, 1951).
3. J. R. Pierce, IRE Trans. Electron Devices ED-3, 183 (1956).
4. O. Buneman, J. Electron. Control 3, 1,507 (1957).
5. O. Buneman, in Crossed-Field Microwave Devices, E. Okress, ed. (Academic Press, New York, 1961), Vol. 1, pp. 209ff and 367ff.
6. R. H. Levy, Phys. Fluids 8, 1288 (1965).
7. O. Buneman, R. H. Levy and L. M. Linson, J. Appl. Phys. 37, 3203 (1966).
8. C. E. Nielsen, A. M. Sessler and K. R. Symon, in Proc, Intl. Conf. on High-Energy Accelerators and Instrumentation (Geneva), p. 239, (1959).
9. A. A. Kolomenskii and A. N. Lebedev, ibid., p. 115.
10. R. J. Briggs and V. K. Neil, J. Nucl. Energy C9, 209 (1967).
11. R. W. Landau and V. K. Neil, Phys. Fluids 9, 2412 (1966).
12. J. D. Callen and C. W. Horton, Phys. Fluids 13, 154 (1970).
13. R. W. Landau, Phys. Fluids 11, 205 (1968).
14. R. Q. Twiss, Aust. J. Phys. 11, 564 (1958).
15. J. Schneider, Phys. Rev. Lett. 2, 504 (1959).
16. A. V. Gaponov, Izu. VUZ., Radiofizika 2, 450 (1959) and addendum, ibid., p. 836.
17. Some suggested review articles are:

    J. L. Hirshfield and V. L. Granatstein, IEEE Trans. Microwave Theory Tech. MTT-25, 522 (1977).

    V. A. Flyagin, A. V. Gaponov, M. I. Petelin and V. K. Yulpatov, ibid., p. 514.

    P. Sprangle and A. T. Drobot, ibid., p. 528.

A. A. Andronov, et. al., Infrared Phys. 18, 385 (1978).

J. L. Hirshfield in Infrared and Millimeter Waves Vol. I, K. J. Button, ed. (Academic Press, New York, 1979) pp. 1-54.

R. S. Symons and H. R. Jory in Advances in Electronics and Electron Physics Vol. 55, C. Marton, ed. (Academic Press, New York, 1981).

V. L. Granatstein, M. Read and L. R. Barnett., Inter. J. Infrared and Millimeter Waves, 5 (1982).

Y. Y. Lau, IEEE Trans. Electron Devices 29, 320 (1982).

18. Y. Y. Lau, (to appear in IEEE Trans. Electron Devices, March 1984).

19. N. Rostoker, Part. Accel. 5, 93 (1973).

20. C. A. Kapetanakos, P. Sprangle, D. P. Chernin, S. J. Marsh and I. Haber, Phys. Fluids 26, 1634 (1983).

21. J. M. Finn and W. M. Manheimer, Phys. Fluids 26, 3400 (1983).

22. P. Sprangle and D. Chernin, Part. Accel. (in press).

23. N. C. Christofilos in Proc. of the Second Intl. Conf. on the Peaceful Uses of Atomic Energy (Geneva) Vol. 32, p. 279, (1958).

24. I. Alexeff and F. Dyer, Phys. Rev. Lett. 43, 351 (1980). See also, L. R. Barnett, doctoral dissertation, Univ. of Tennessee, Knoxville (1978), for a related device.

25. G. Dohler, submitted to IEEE Trans. Electron Devices (1983).

26. R. H. Pantell, IRE Trans. Electron Devices ED-7, 22 (1960).

27. Some analytical and numerical work, with different applications in mind, has been reported by B. Godfrey, IEEE Trans. Plasma Sci. PS-7, (1979).

28. Y. Y. Lau and D. Chernin, to appear in Phys. Rev. Lett. (1984).

29. R. C. Davidson and K. Tsang, Bull. Am. Phys. Soc. 28, 1211 (1983).

30. Y. Y. Lau and R. J. Briggs, Phys. Fluids 14, 967 (1971).

31. It is also possible, of course, to expand the eigenfunction ϕ about any of the singularities of Eq. (14). If this is done for the longitudinal mode an expression similar to Eq. (26) but containing certain logarithmic terms is obtained; these log terms may be shown to be stabilizing. Such an expansion about $\Omega = 0$ was used to obtain the second order term given in Eq. (36). Of course if both series, about $r = R$ and about $\Omega = 0$, are convergent then they must give identical results for the dispersion relation. We should point out that the transverse modes may also be studied via an expansion about the mid point $r = (r_1 + r_2)/2$, whereas an expansion about $\Omega = 0$ focuses only on the longitudinal modes.

32. R. J. Briggs and V. K. Neil, J. Nucl. Energy C8, 255 (1966).

33. J. Swegle and E. Ott, Phys. Fluids 24, 1821 (1981); also, J. Swegle, Phys. Fluids 26, 1670 (1983).

34. D. Chernin, Phys. Fluids 25, 1342 (1982).

35. V. K. Neil and A. M. Sessler, Rev. Sci. Instr. 36, 429 (1965).

36. L. S. Laslett, V. K. Neil and A. M. Sessler, Rev. Sci. Instr. 36, 436 (1965).

37. C. L. Chang, T. M. Antonsen, Jr., E. Ott and A. T. Drobot, submitted to Phys. Fluids (1983).

38. V. K. Neil and W. Heckrotte, J. Appl. Phys. 36, 2761 (1965).

39. M. A. Mostrom and M. E. Jones, Phys. Fluids 26, 1649 (1983).

Figure Captions

Fig. 1. Model of an E-layer. The layer, of infinite extent in z (in and out of the page), occupies the region $r_1 < r < r_2$ between the walls of a coaxial guide at r=a and r=b. The electrons, supported by an electric field $E_o(r)\hat{r}$ and a magnetic field $B_o(r)\hat{z}$, move in concentric circles in the equilibrium state, either clockwise or counterclockwise depending on the equilibrium type.

Fig. 2. The $\alpha_E - \alpha_B$ plane. The number and type of solutions to the equation of radial force balance (6) are shown in each region and on the boundaries between regions. A root is labeled + or - if it corresponds to clockwise or counterclockwise rotation respectively as one looks in the direction of $\hat{B}_o$.

Fig. 3. Plot of the dimensionless "azimuthal mass" M versus the dimensionless equilibrium electric field, h. The actual plot shown is for the case $\gamma_o = 1.5$ but all axis labels are expressed generally in terms of γ_o or β_o.

Fig. 4. Normalized growth rate for the negative mass instability versus h for the case a = 0.6m, b = 2.6m, R = 1.0m, $\tau/R = 0.02$, $\gamma_o = 1.5$, $\ell = 1$. A solid curve indicates data obtained from a numerical solution of Eq. (14); the dashed line is a plot of Eq. (31). The upper pair of curves is for $\nu/\gamma_o = 7.88 \times 10^{-3}$, $\xi = 1.42$; the lower pair is for $\nu/\gamma_o = 1.57 \times 10^{-3}$, $\xi = 0.28$.

Fig. 5. Normalized growth rate for the negative mass instability versus ν/γ_o for the "base case" parameters: $a = 0.5m$, $b = 2.2m$, $r_1 = 0.99m$, $r_2 = 1.01m$, $\gamma_o = 3$, $\ell = 1$. A solid curve denotes data obtained from a numerical solution of the eigenvalue problem; a dashed curve denotes data from the dispersion relation, Eq. (31).

Fig. 6. Normalized growth rate for the negative mass instability versus layer thickness. All parameters take their base case values, (see text) except that the peak density in the parabolic profile is 10^7/cc.

Fig. 7. Normalized growth rate for the negative mass instability versus outer wall position. All parameters take their base case values. (See text.) Near synchronous conditions, $\ell\omega_o \approx \omega_v$ where ω_v is a waveguide mode satisfying $b_+ + b_- = 0$, the negative mass instability is strongly enhanced and Eq. (31) should be solved as a cubic polynomial. The synchronous or enhanced negative mass instability is often called the cyclotron maser instability.

Fig. 8. Normalized growth rate for the negative mass instability versus inner wall position. All parameters take their base case values. (See text.)

Fig. 9. Normalized growth rate for the negative mass instability versus γ_o. All parameters take their base case values, (see text) except that the peak density in the parabolic profile is 10^8/cc.

Fig. 10. Normalized growth rate for the negative mass instability versus azimuthal mode number ℓ. All parameters take their base case values. (See text.) A + denotes a result from Eq. (31) and an × denotes a result from a numerical solution of the eigenvalue problem.

Fig. B-1. Normalized admittances vs. outer wall position for various inner wall positions for $\ell = 1$ and $mc^2(\gamma_o - 1) = 1$ keV.

Fig. B-2. As in Fig. B-1 but for $mc^2(\gamma_o - 1) = 5$ keV.

Fig. B-3. As in Fig. B-1 but for $mc^2(\gamma_o - 1) = 40$ keV.

Fig. B-4. As in Fig. B-1 but for $mc^2(\gamma_o - 1) = 300$ keV. The zeroes of $b_+ + b_-$ correspond to waveguide cutoff frequencies.

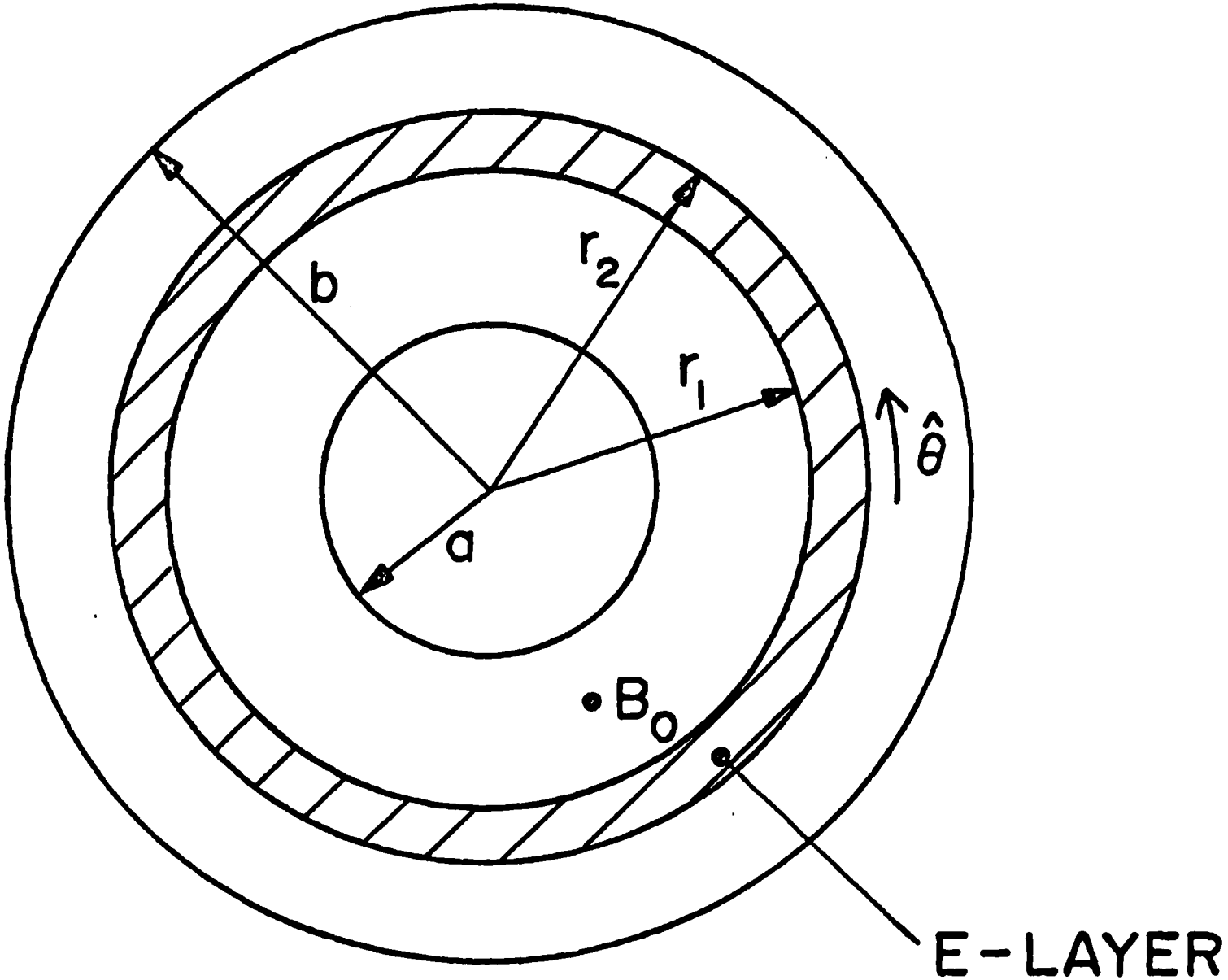

FIGURE 1

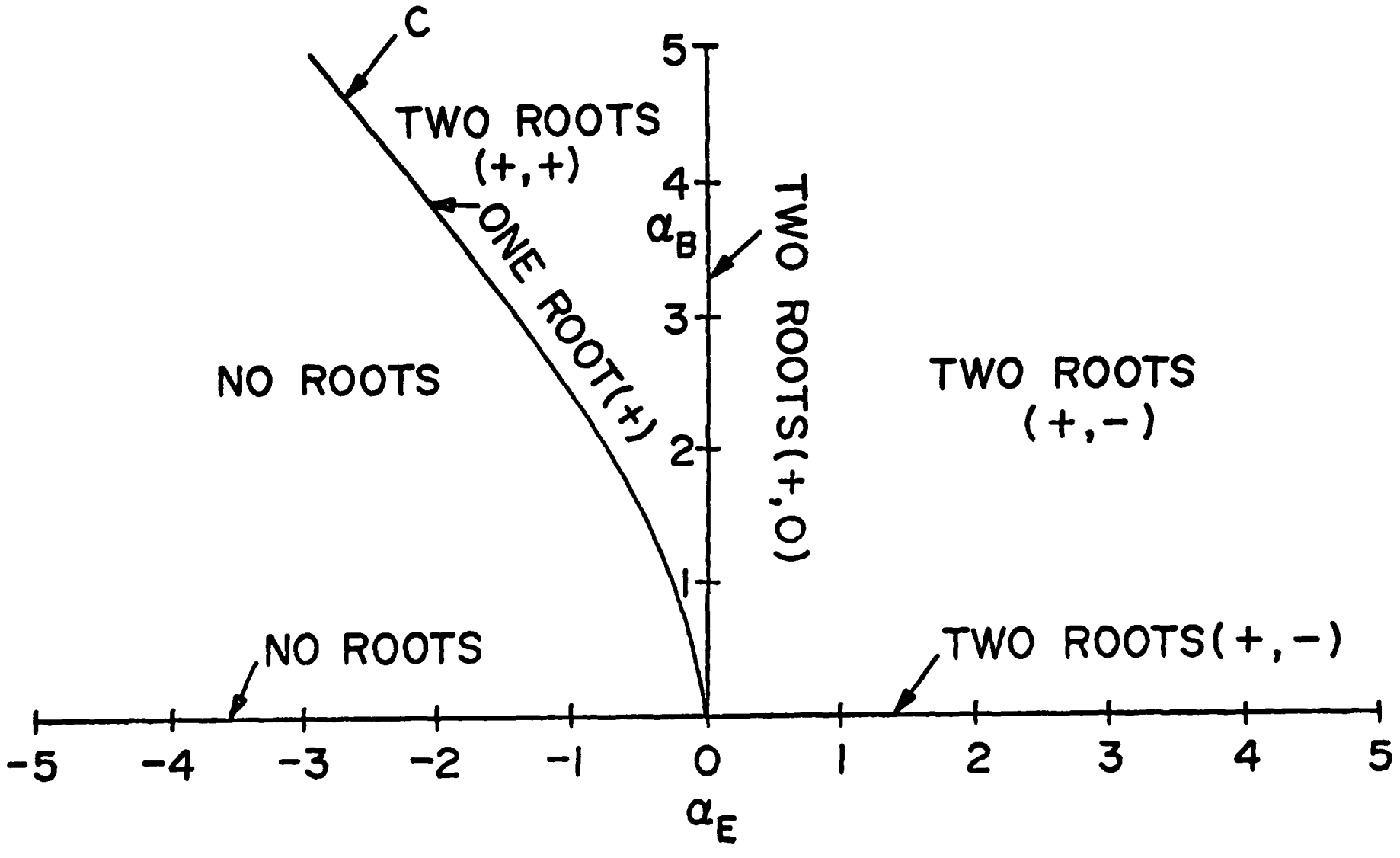
C
TWO ROOTS
(+,+)
ONE ROOT(+)
TWO ROOTS(+,0)
NO ROOTS
TWO ROOTS
(+,-)
NO ROOTS
TWO ROOTS(+,-)
5
4
3
2
1
α_B
-5
-4
-3
-2
-1
0
1
2
3
4
5
α_E

FIGURE 2

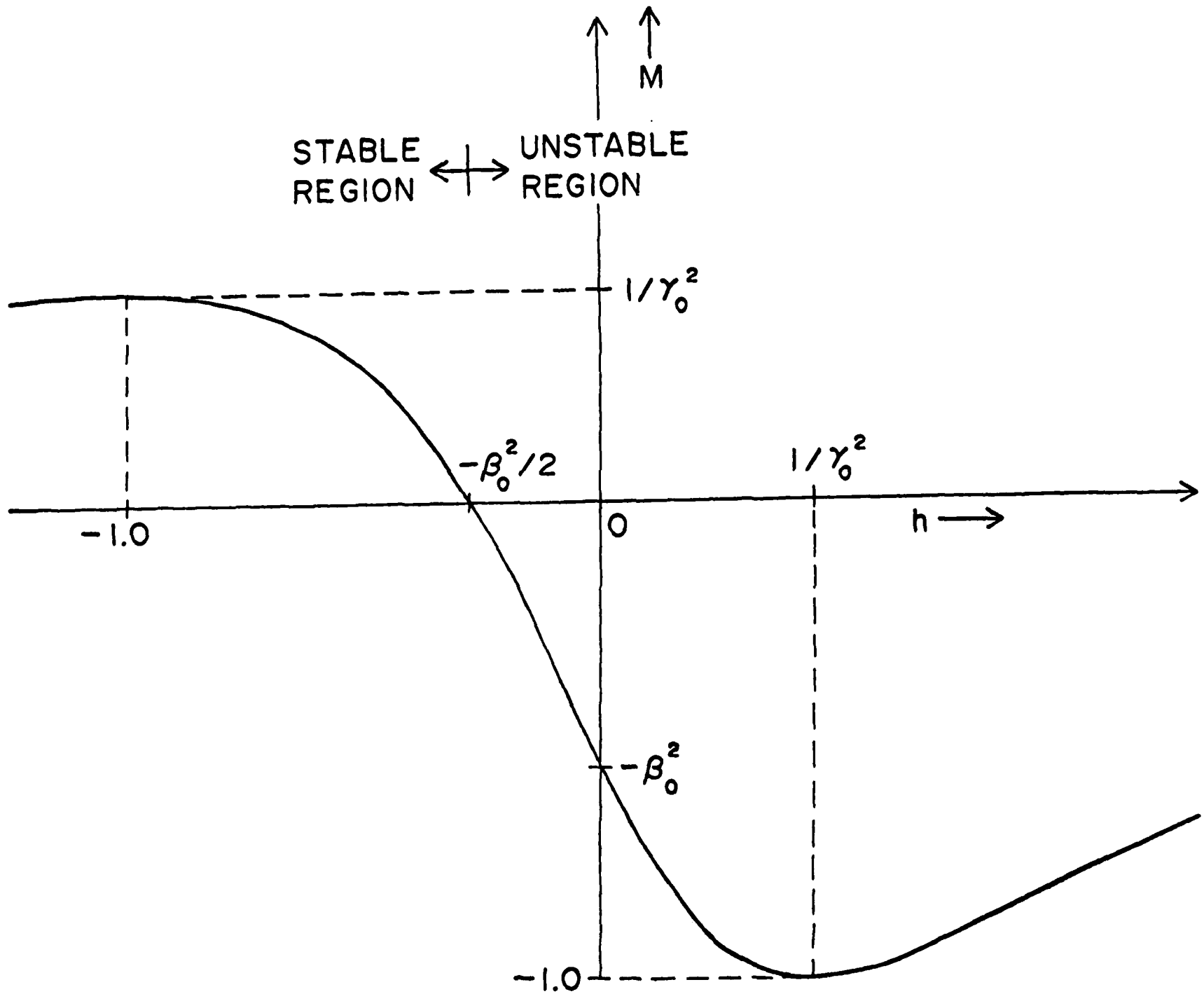
M
STABLE REGION
UNSTABLE REGION
$1/\gamma_0^2$
$-\beta_0^2/2$
$1/\gamma_0^2$
-1.0
0
h
$-\beta_0^2$
-1.0

FIGURE 3

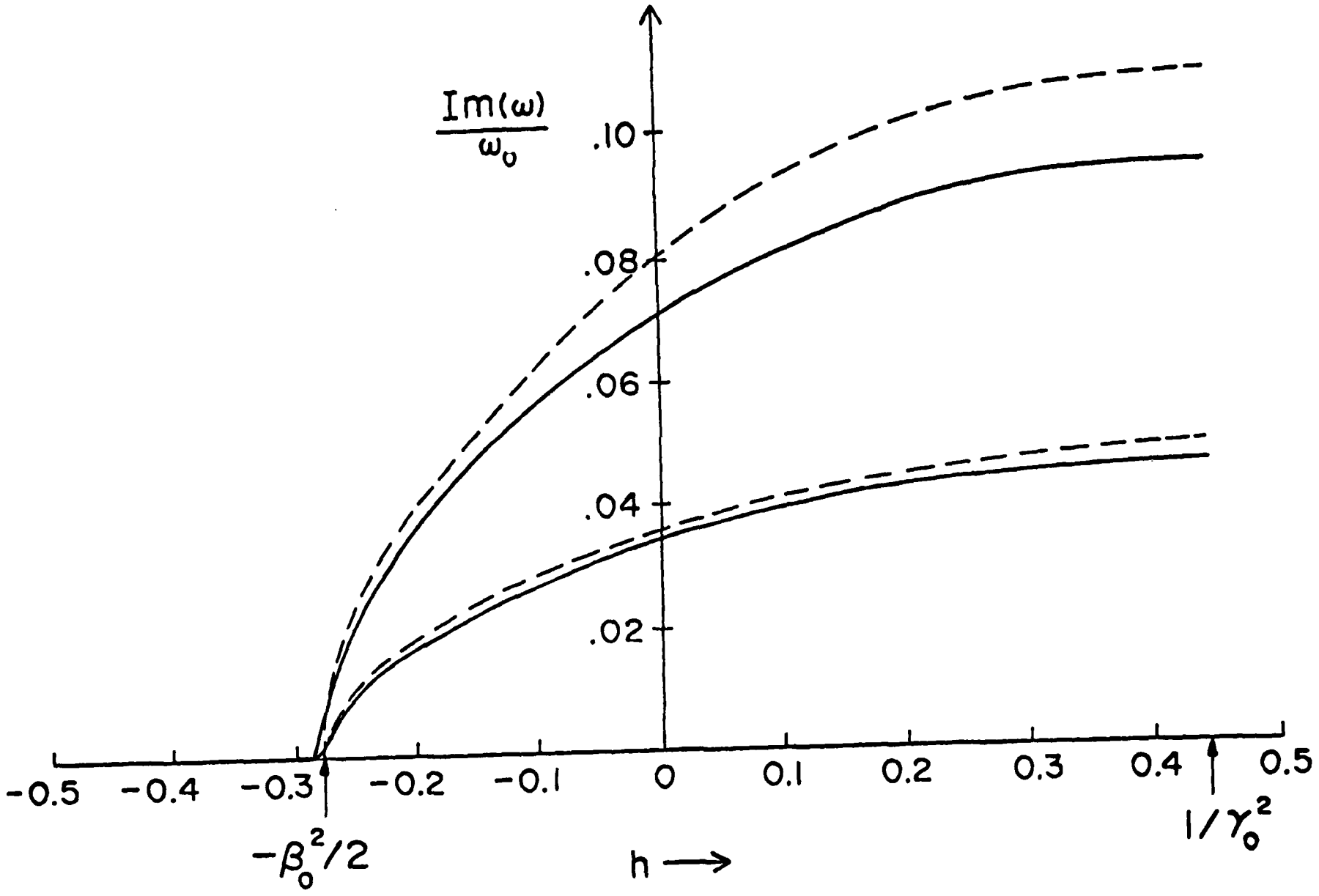

FIGURE 4

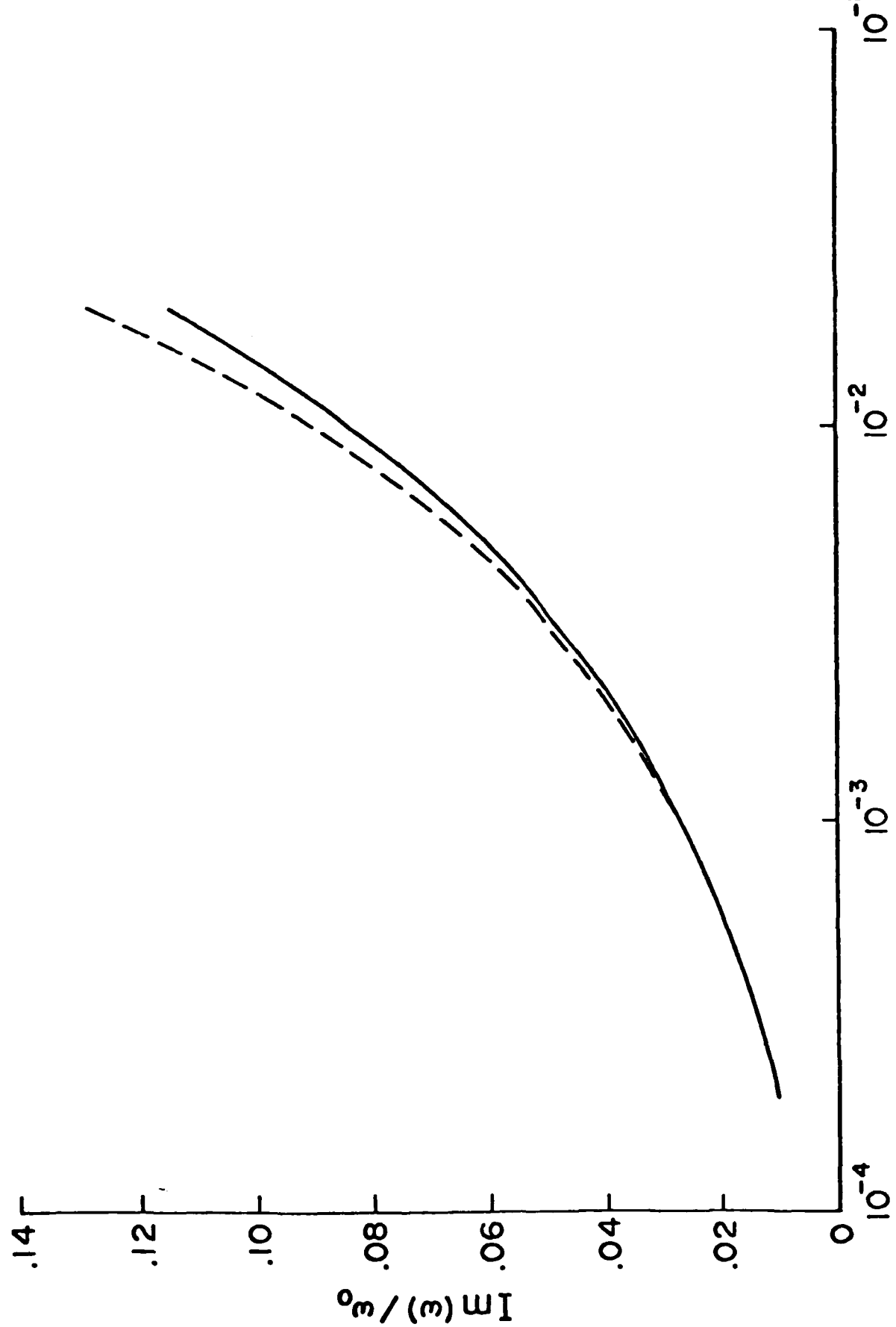

FIGURE 5

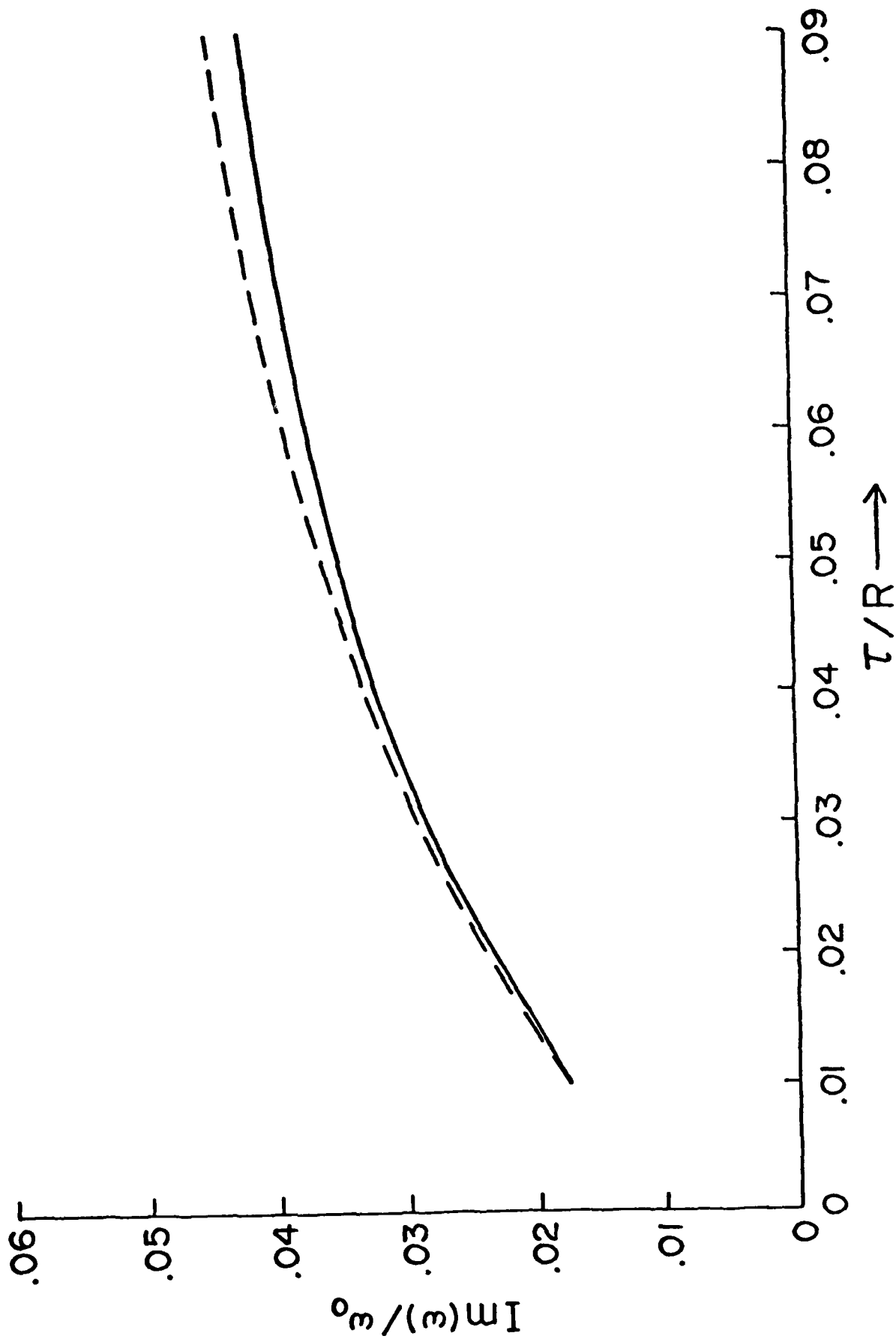

FIGURE 6

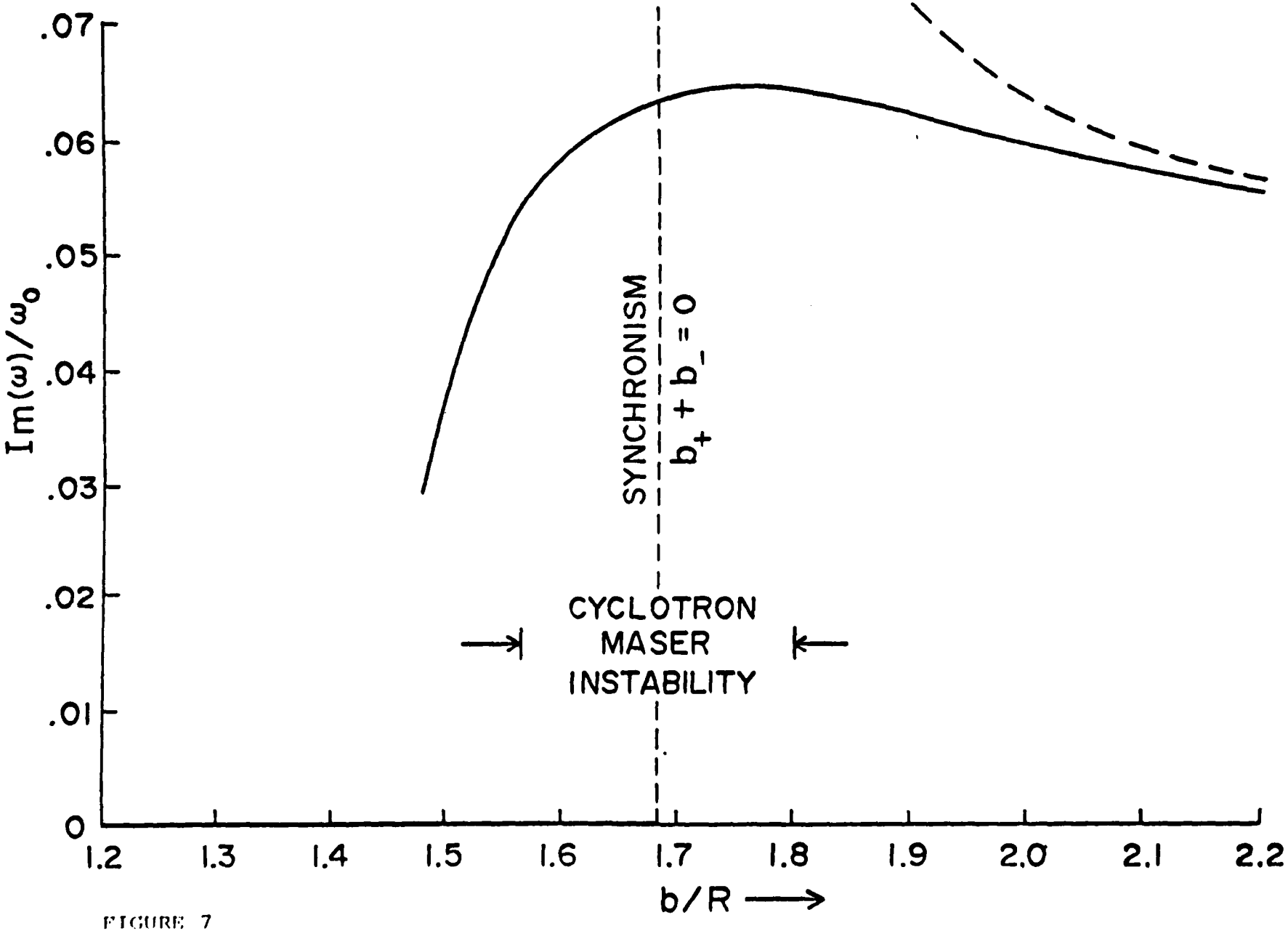
.07
.06
.05
.04
.03
.02
.01
0
Im(ω)/ω₀
SYNCHRONISM
b₊ + b₋ = 0
CYCLOTRON
MASER
INSTABILITY
1.2
1.3
1.4
1.5
1.6
1.7
1.8
1.9
2.0
2.1
2.2
b/R ⟶

FIGURE 7

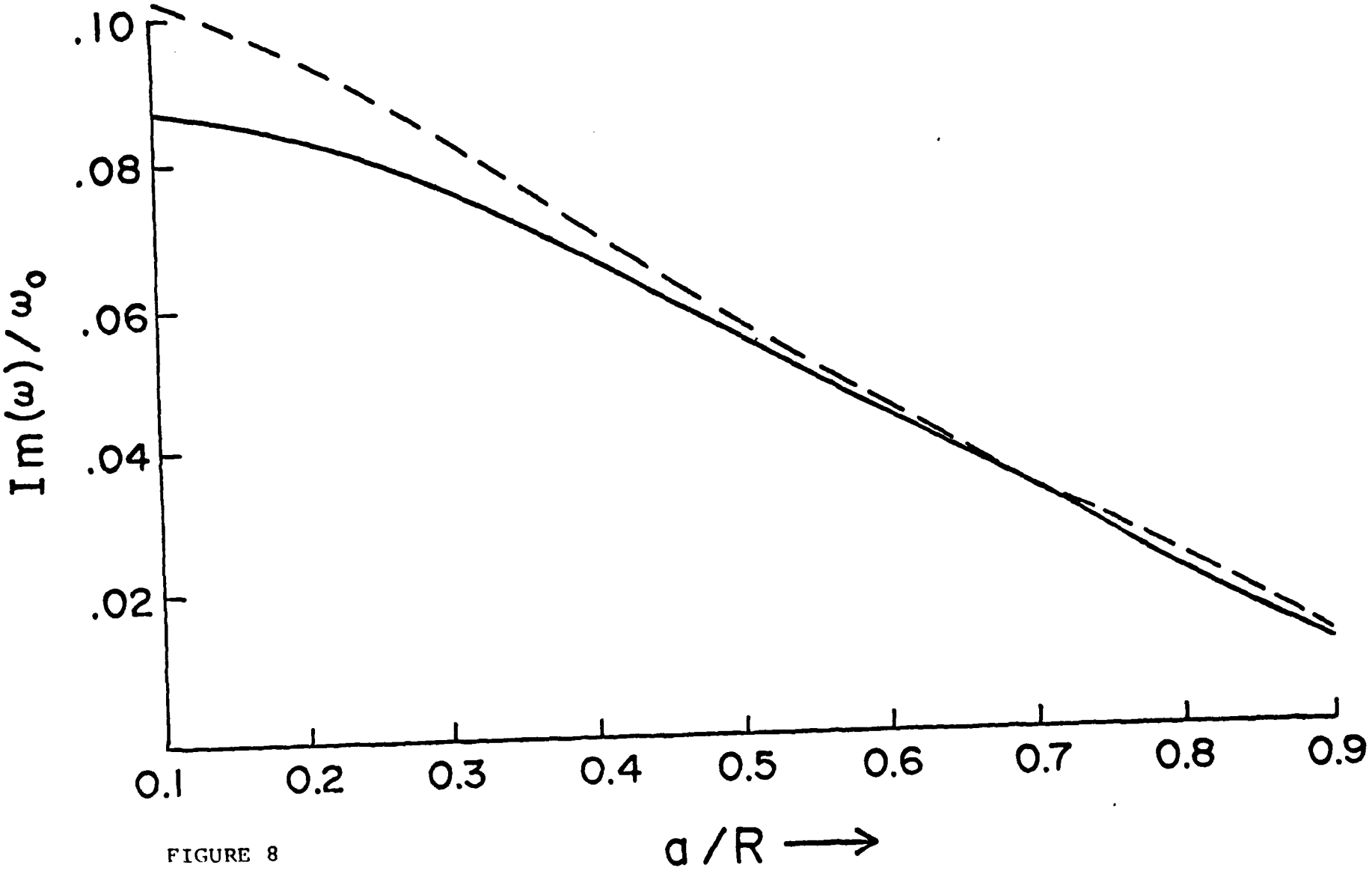

FIGURE 8

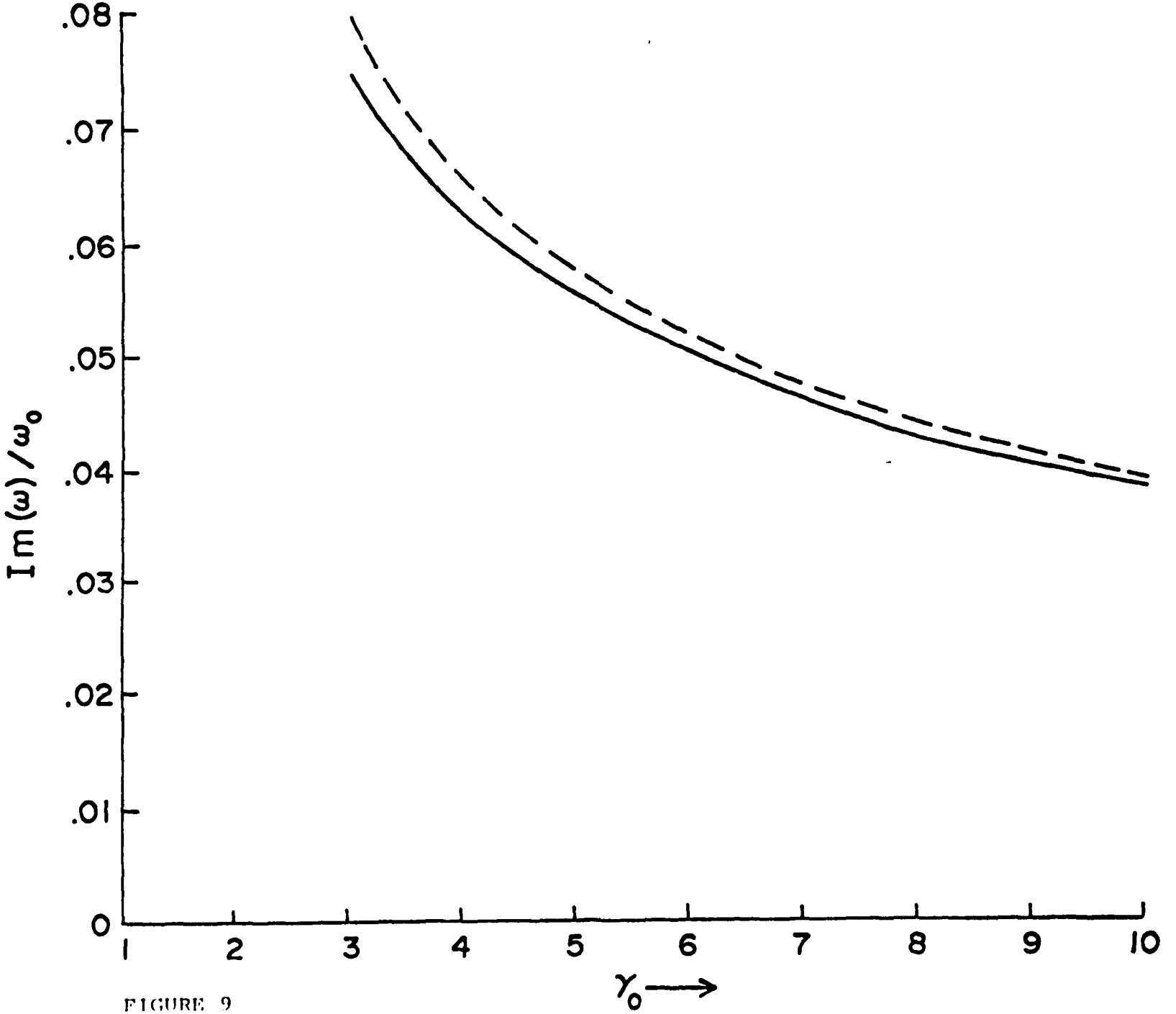

FIGURE 9

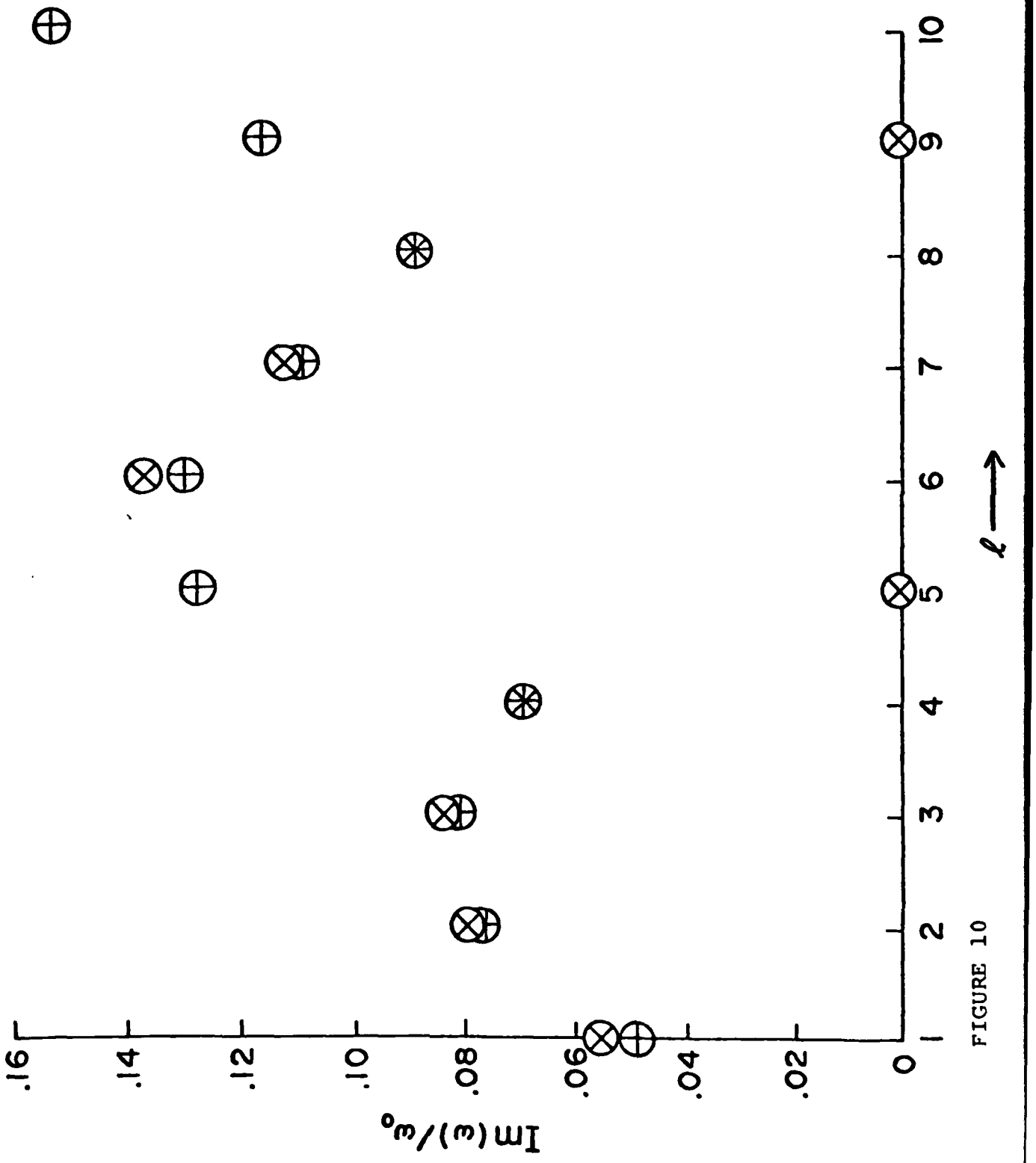

FIGURE 10

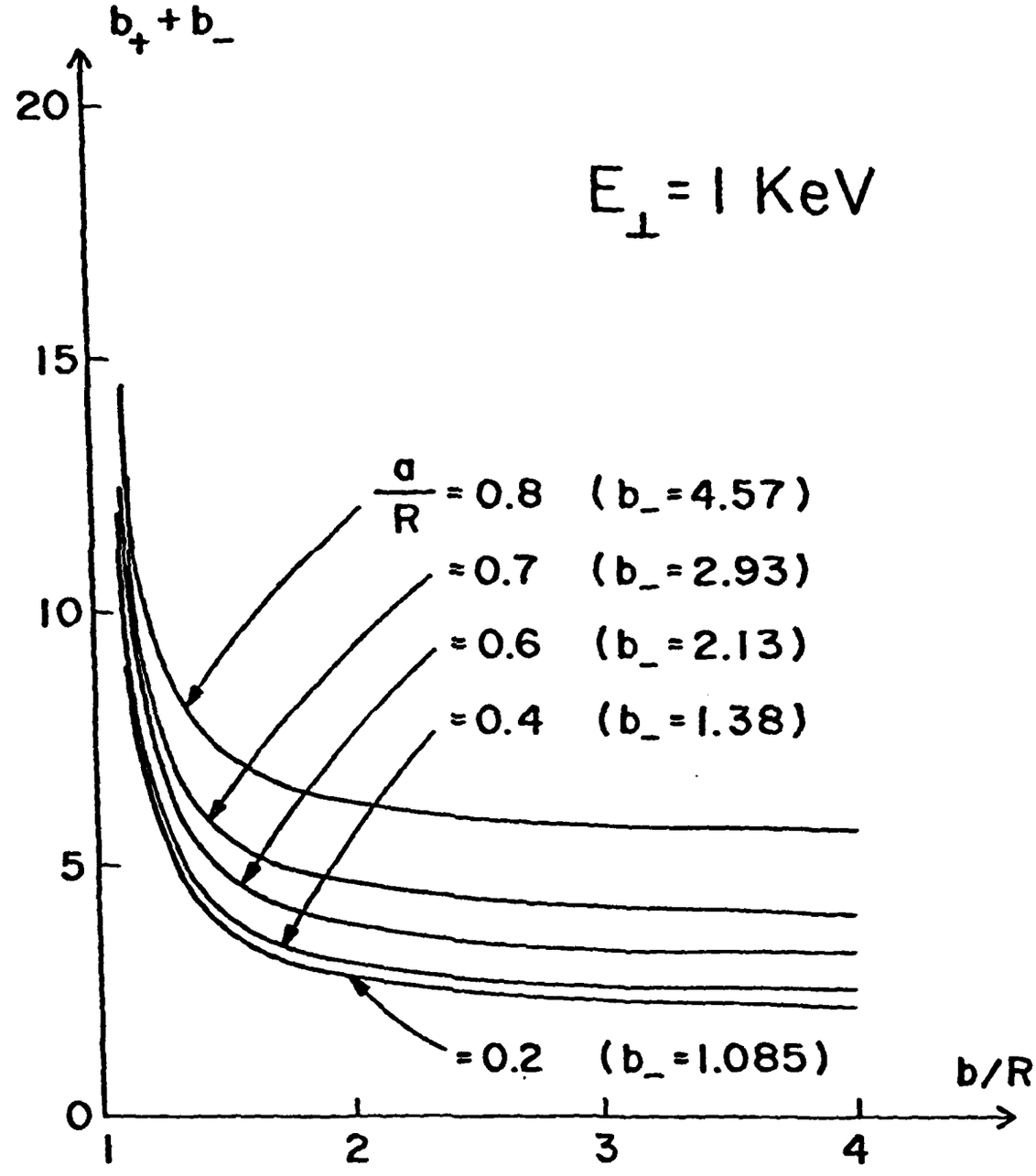
$b_+ + b_-$
20
15
10
5
0
1
2
3
4
b/R
$E_\perp = 1$ KeV
$\frac{a}{R} = 0.8$ ($b_- = 4.57$)
$= 0.7$ ($b_- = 2.93$)
$= 0.6$ ($b_- = 2.13$)
$= 0.4$ ($b_- = 1.38$)
$= 0.2$ ($b_- = 1.085$)

FIGURE B-1

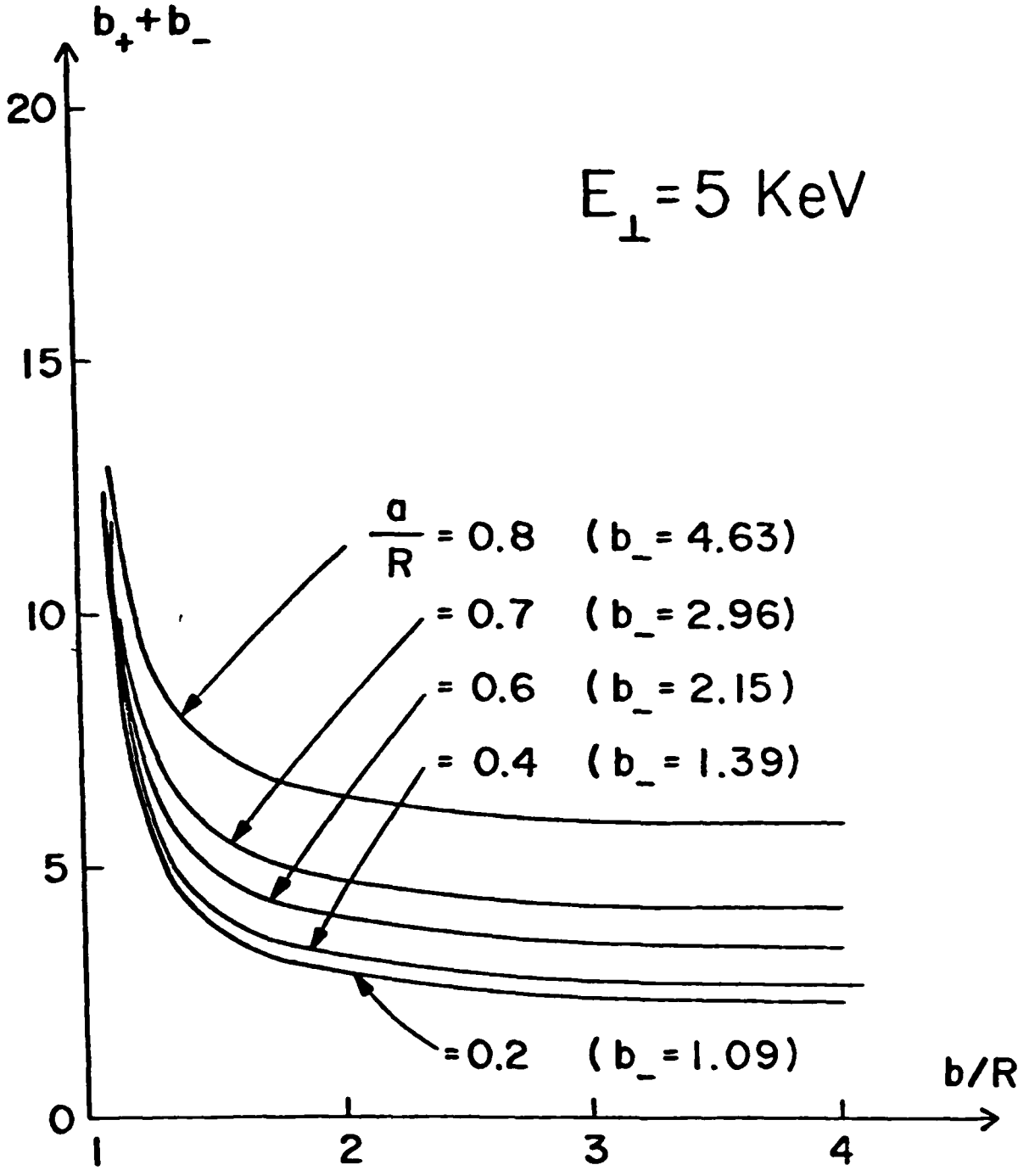
$b_+ + b_-$
20
15
10
5
0
1
2
3
4
b/R
$E_\perp = 5$ KeV
$\frac{a}{R} = 0.8$ ($b_- = 4.63$)
$= 0.7$ ($b_- = 2.96$)
$= 0.6$ ($b_- = 2.15$)
$= 0.4$ ($b_- = 1.39$)
$= 0.2$ ($b_- = 1.09$)

FIGURE B-2

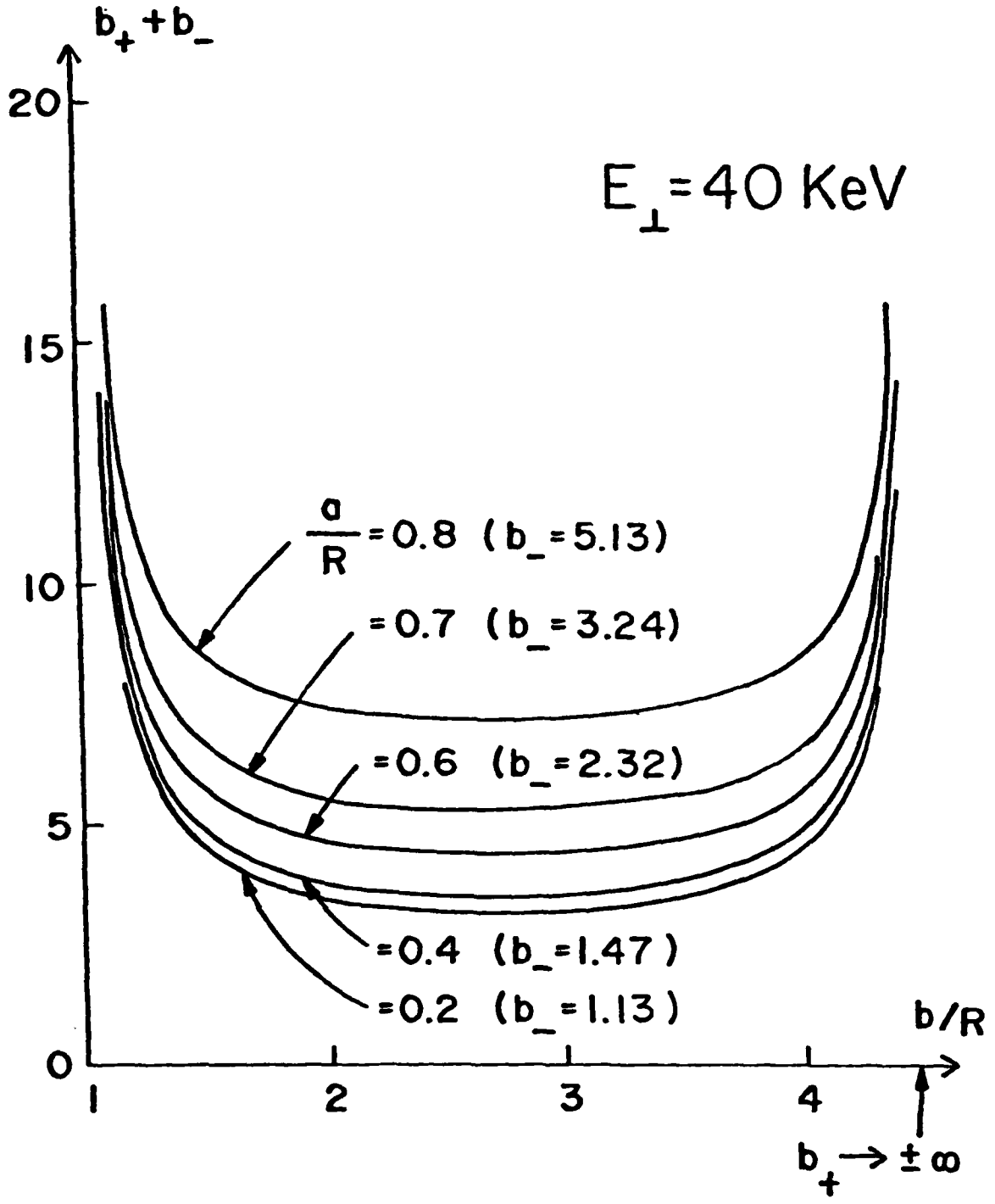
b+ + b-
20
15
10
5
0
E⊥ = 40 KeV
a/R = 0.8 (b- = 5.13)
= 0.7 (b- = 3.24)
= 0.6 (b- = 2.32)
= 0.4 (b- = 1.47)
= 0.2 (b- = 1.13)
b/R
1
2
3
4
b+ → ±∞

FIGURE B-3

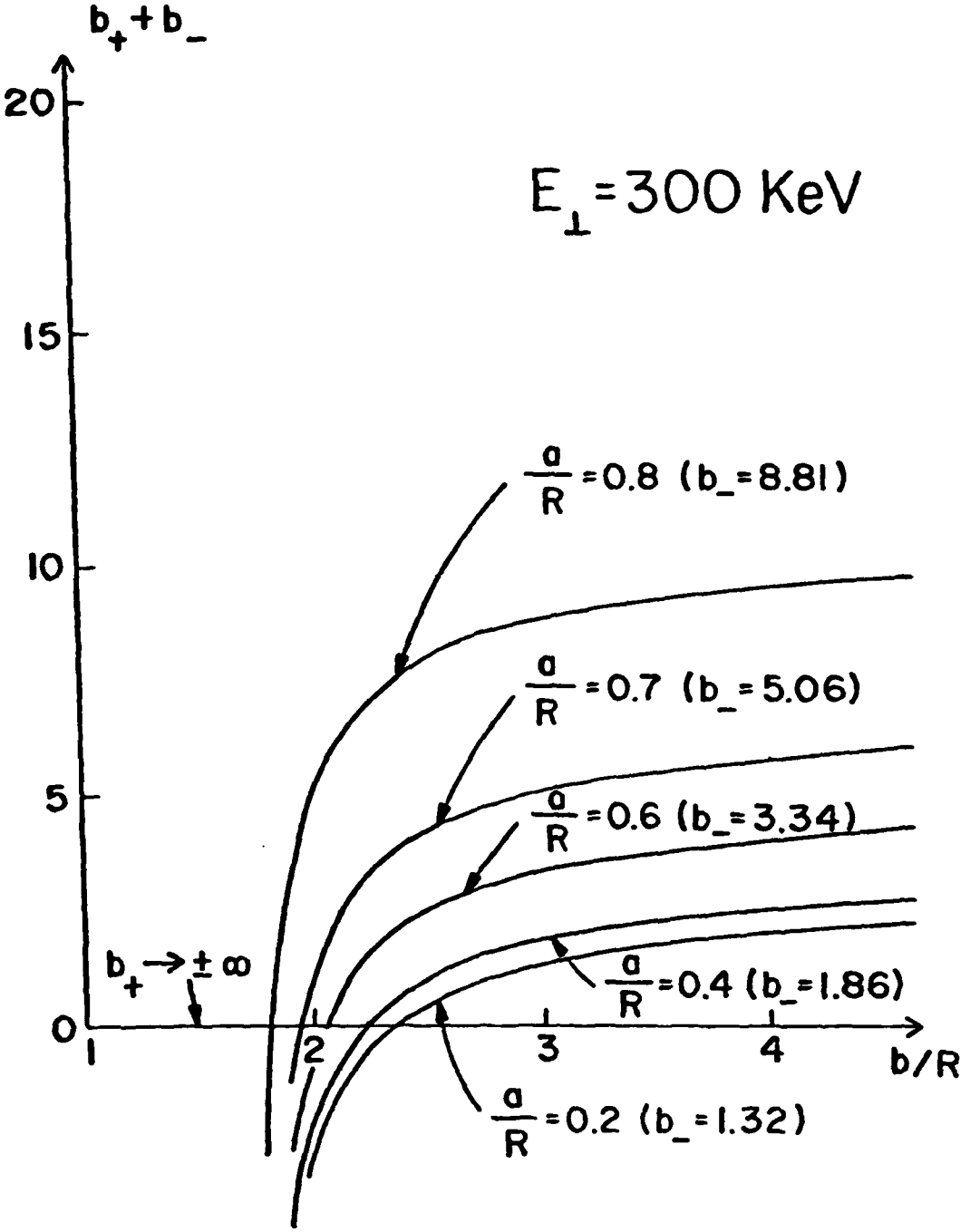
$b_+ + b_-$
20
15
10
5
0
$E_\perp = 300$ KeV
$\frac{a}{R} = 0.8$ ($b_- = 8.81$)
$\frac{a}{R} = 0.7$ ($b_- = 5.06$)
$\frac{a}{R} = 0.6$ ($b_- = 3.34$)
$\frac{a}{R} = 0.4$ ($b_- = 1.86$)
$\frac{a}{R} = 0.2$ ($b_- = 1.32$)
$b_+ \rightarrow \pm\infty$
1
2
3
4
b/R

FIGURE B-4

APPENDIX C

Program ASTRON

Program ASTRON

Input data file: FORØ15.DAT (free format)

All quantities in MKS units

100	...	: Label
200	a,b	: Inner, outer cylinder radii
300	r_1, r_2	: Inner, outer beam radii
400	n_{oo}, pwr	: Peak number density, power (Note 1)
500	$\phi_o(b)$, B_{oo}	: Bias potential at r = b; Applied B field
600	KBR	: (+1,-1) = (greater, lesser) of two roots of eqn. of motion
700	ε_1, ε_2	: Error allowed in calculating $U(r_1)$; $H_o(r_1)$
800	I1	: If = 1, write equilibrium quantities to file FORØ2Ø.DAT
900	IEV	: (0,1) = (stop, continue) after calculation of equilibrium
1000	...	: Label
1100	ZW,L	: Initial guess for $\omega/\omega(r_1)$, azimuthal mode number
1200	KT1, KT2, KT3	: Number of calls to integration package in $(a \to r_1)$, $(r_1 \to r_2)$, $(r_2 \to b)$ respectively
1300	TOL, ε_3	: Integration error control; error control for eigenvalue convergence test
1400	I2, I3	: I2 = 1 ⇒ Write eigenfunction to file FORØ22.DAT I3 = 1 ⇒ Write $(\omega - \ell\omega_o(r))/\omega_o(r_1)$ and d to file FORØ24.DAT.

Note 1: Functional form of density is taken as

$$n = n_{oo}\left[\frac{4(r_2-r)(r-r_1)}{(r_2-r_1)^2}\right]^{pwr}$$

Output data files: (All binary)

Equilibrium quantities:

FORØ2Ø.DAT: r, E_o, H_o, u, ξ, h, $mc^2\omega_o'/(\omega_o\varepsilon')$ for $r = r_1$ to r_2.

Eigenfunction:

FORØ22.DAT: r, Re($rE_{\theta 1}$), Im($rE_{\theta 1}$) for r = a to b.

Singularity locations:

FORØ24.DAT: r, Re $((\omega-\ell\omega_o(r))/\omega_o(r_1))$, Re(d), Im(d)

```
type astroncom.for
C       COMMON CODE FOR PROGRAM ASTRON
        IMPLICIT REAL*8(A-H,O-R,T-Y)
        IMPLICIT COMPLEX*16 Z
        PARAMETER(N1=200)
C       N1 MUST BE EVEN
        COMMON/GEOM/A,B,R1,R2,R2R1
        COMMON/CNTRL/N,DR,DR2,NBR,EPS1,EPS2,IEV
        COMMON/DEN/DEN0,PWR,T22,G00
        COMMON/BIAS/PHIOB,B00
        COMMON/CONST/QE,EM,EPS0,XMU0,C,QEMC2
        COMMON/FIELDS/E0(0:N1),H0(0:N1)
        COMMON/PARTS/U(0:N1)
        COMMON/DVDHM/DM(0:N1)
        COMMON/NORM/B01,B012,DRH01,DRH02,DRH03,DDRH0
        COMMON/CNTRL2/NT1,NT2,NT3,TOL,EPS3
        COMMON/EV/ZW,EL,EL2
        COMMON/ADMITS/ZBPLUS,ZBMINUS
        COMMON/COEF/ZMAT(4,4)
        COMMON/EQUIL/XI(0:N1),HG(0:N1),W0B(0:N1)
        COMMON/OUTS/I1,I2,I3
        DATA QE,EM,EPS0,XMU0,C
     1  /1.6023D-19,9.1095D-31,8.8543D-12,12.5664D-7,2.9979D8/
        DATA QEMC2/1.9571D-6/
        DATA ZMAT/16*(0.D0,0.D0)/
$
```

```
type astr...forastron.for
      PROGRAM ASTRON
      INCLUDE 'ASTRONCOM.FOR'
      REWIND 20
      N=N1
      CALL INPUT1
      CALL ECAL
      CALL HVCAL
      PRINT10
10    FORMAT(/,' EQUILIBRIUM CALCULATION COMPLETED',/)
      B01=U(0)/DSQRT(U(0)**2+1.D0)
      B012=B01**2
      G00=DSQRT(U(N/2)**2+1.D0)
      WOR1=B01*C/R1
      DO100 NN=0,N
      R=R1+DFLOAT(NN)*DR
      U2=U(NN)**2
      GMA=DSQRT(U2+1.D0)
      XI(NN)=QEMC2*EDEN(R)*R*GMA/U2
      HG(NN)=QEMC2*EO(NN)*R/U2
      WOR(NN)=C*U(NN)/(GMA*R*WOR1)
      IF(I1.EQ.1)THEN
      H=HG(NN)/GMA
      GMA2=GMA**2
      GMA4=GMA2**2
      BETA2=1.D0-1.D0/GMA2
      DWDE=-(BETA2+2.D0*H+XI(NN)/GMA4)/
     1 (GMA*BETA2*(1.D0-XI(NN)/GMA2+HG(NN)**2))
      WRITE(20)SNGL(R),SNGL(EO(NN)),SNGL(HO(NN)),SNGL(U(NN)),
     1 SNGL(XI(NN)),SNGL(H),SNGL(DWDE)
      ENDIF
100   CONTINUE
      XIAV=DSIMP(4)/(R2-R1)
      ENS=DSIMP(5)/(R2-R1)
      FNORM=DSIMP(6)
      UAV=DSIMP(7)/FNORM
      U2AV=DSIMP(8)/FNORM
      WAV=DSIMP(9)/FNORM
      W2AV=DSIMP(10)/FNORM
      XNUG=0.5D0*B012*DSIMP(11)/(R1**2)
      DELU=DSQRT(12.D0*(U2AV-UAV**2))/UAV
      DELW=DSQRT(12.D0*(W2AV-WAV**2))/WAV
      GAV=DSQRT(1.D0+UAV**2)
      PRINT20,XNUG,XIAV,ENS,UAV,GAV,DELU,DELW,WOR1
20    FORMAT(' NU/GAMMA=',1PD10.3,/,
     1 ' AVERAGE VALUE OF (PLASMA FREQ/CIRC FREQ)**2=',0PF10.4,/,
     2 ' AVERAGE VALUE OF SELF FIELD INDEX (NS)=',F10.4,/,
     3 ' DENSITY WEIGHTED AVERAGE OF BETA*GAMMA=',F10.4,/,
     4 ' (CORRESPONDING GAMMA=',F10.4,')',/,
     5 ' FRACTIONAL LINEAR MOMENTUM SPREAD=',F10.4,/,
     6 ' FRACTIONAL ANGULAR FREQUENCY SPREAD=',F10.4,/,
     7 ' CIRCULATION FREQ AT R=R1=',1PD10.3,' RAD/SEC')
      CURRL=HO(0)-HO(N)
      PRINT21,CURRL
21    FORMAT(' CURRENT PER UNIT LENGTH=',1PD10.3,' A/M',/)
      IF(IEV.NE.1)GOTO200
      CALL INPUT2
      CALL SHOOTER
      ZBPM=ZBPLUS+ZBMINUS
      PRINT30,ZBPLUS,ZBMINUS,ZBPM
30    FORMAT(//,' B+ =',1PD12.4,/,' B- =',D12.4,/,
     1 ' SUM=',D12.4,/)
      IF(I3.EQ.1)THEN
```

```
      DO110 NN=0,N
      GMA=DSQRT(U(NN)**2+1.D0)
      BET=U(NN)/GMA
      ZOM=ZW-EL*WOB(NN)
      ZOMW=ZOM/WOE(NN)
      RHO=1.D0+DFLOAT(NN)*DDRHO
      R=RHO*R1
      ZT1=1.D0+HG(NN)**2-ZOMW**2
      ZT2=ZW*ZW*RHO*RHO*BO12-EL2
      ZT3=BET*BO1*ZW*RHO-EL
      ZD=ZT1*ZT2+XI(NN)*ZT3**2
      S1=R
      S2=DREAL(ZOM)
      S3=DREAL(ZD)
      S4=DIMAG(ZD)
      WRITE(24)S1,S2,S3,S4
110   CONTINUE
      ENDIF
200   CONTINUE
      STOP
      END
      SUBROUTINE INPUT1
      INCLUDE 'ASTRONCOM.FOR'
      READ(15,*)
      READ(15,*)A,B
      READ(15,*)R1,R2
      T22=((R2-R1)/2.D0)**2
      DR=(R2-R1)/DFLOAT(N)
      DR2=DR/2.D0
      READ(15,*)DENO,PWR
      READ(15,*)PHIOB,BOO
      READ(15,*)XBR
      READ(15,*)EPS1,EPS2
      READ(15,*)I1
      READ(15,*)IEV
      RETURN
      END
      SUBROUTINE ECAL
      INCLUDE 'ASTRONCOM.FOR'
      ELBA=DLOG(B/A)
      C1=(PHIOB+DSIMP(1))/ELBA
      EO(0)=-C1/R1
      P=0.D0
      R=R1
      DO10 NN=1,N
      P=P+(EDEN(R)+EDEN(R+DR)+4.D0*EDEN(R+DR2))*DR2/3.D0
      R=R+DR
10    EO(NN)=-(C1+P)/R
      RETURN
      END
      SUBROUTINE HVCAL
      INCLUDE 'ASTRONCOM.FOR'
      AAE=QE*EO(0)*R1/(EM*C*C)
      B2A2=B**2-A**2
      AAH1=QE*BOO*0.5D0*(R1+R2)/(EM*C)
      BETA1=AAH1/DSQRT(1.D0+AAH1**2)
      HOOM=BOO/XMUO
      HOM=HOOM+C*BETA1*DSIMP(3)/B2A2
      LH=0
1     CONTINUE
      PRINT2,HOM
2     FORMAT(' HOM= ',1PD10.3)
      AAH=QE*XMUO*HOM*R1/(EM*C)
```

```
      CALL UROOTS(UM,AAE,AAH)
      U(0)=UM
C     INTEGRATION OF U EQUATION
      DO20 NN=0,N-1
      Y=U(NN)
      R=R1+DFLOAT(NN)*DR
      E=EO(NN)
      F1=UPRM(R,Y,E)
      E=(EO(NN)+EO(NN+1))/2.D0
      F2=UPRM(R+DR2,Y+DR2*F1,E)
      F3=UPRM(R+DR2,Y+DR2*F2,E)
      E=EO(NN+1)
      F4=UPRM(R+DR,Y+DR*F3,E)
20    U(NN+1)=Y+(F1+2.D0*(F2+F3)+F4)*DR/6.D0
C     CALCULATION OF U ARRAY COMPLETED
C     CALCULATE XI AND HG ARRAYS
      DO 22 NN=0,N
      R=R1+DFLOAT(NN)*DR
      U2=U(NN)**2
      GMA=DSQRT(U2+1.D0)
      XI(NN)=QEMC2*EDEN(R)*R*GMA/U2
22    HG(NN)=QEMC2*EO(NN)*R/U2
C     CALCULATE SOLUTION FOR DVO/DHO-
      GMA=DSQRT(U(0)**2+1.D0)
      DM(0)=HOM*QE*XMU0*R1/(EM*C*(GMA**2)*(GMA+HG(0)))
      QQR1=DM(0)
      DO24 NN=0,N-1
      QQR0=QQR1
      QQR1=QQR(NN+1)
24    DM(NN+1)=DM(NN)*DEXP(0.5D0*(QQR0+QQR1)*DR)
      FS=HOM/HOOM-DSIMP(2)/(HOOM*B2A2)-1.D0
      HDFS=HOM/HOOM+C*DSIMP(12)/(HOOM*B2A2)
C     ADJUST VALUE FOR HO-
      HOMNEW=HOM*(1.D0-FS/HDFS)
      IF(DABS((HOMNEW-HOM)/HOM).LE.EPS2)GOTO30
      LH=LH+1
      IF(LH.GT.20)STOP 'HOM LOOP CONV FAILURE'
      HOM=HOMNEW
      GOTO1
30    CONTINUE
      PRINT150,LH
150   FORMAT(' HVCAL...FINAL CONV IN',I3,' ITERATIONS',/)
      HO(0)=HOMNEW
      R=R1
      DO40 NN=1,N
      VO=C*U(NN-1)/DSQRT(U(NN-1)**2+1.D0)
      VO1=C*U(NN)/DSQRT(U(NN)**2+1.D0)
      VO2=(VO+VO1)/2.D0
      HO(NN)=HO(NN-1)+EPSO*
     1 (EDEN(R)*VO/R+EDEN(R+DR)*VO1/(R+DR)+4.D0*EDEN(R+DR2)*
     2 VO2/(R+DR2))*DR2/3.D0
      R=R+DR
40    CONTINUE
      RETURN
      END
      FUNCTION DSIMF(J)
      INCLUDE 'ASTRONCOM.FOR'
      ODDS=0.D0
      EVENS=0.D0
      DO 101 NN=1,N-1,2
      R=R1+DFLOAT(NN)*DR
101   ODDS=ODDS+F(J,R)
      DO102 NN=2,N-2,2
```

```
      R=R1+DFLOAT(NN)*DR
102   EVENS=EVENS+F(J,R)
      DSIMF=(F(J,R1)+F(J,R2)+4.D0*DODS+2.D0*EVENS)*DR/3.D0
      RETURN
      END
      FUNCTION F(J,R)
      INCLUDE 'ASTRONCOM.FOR'
      NN=JIDNNT((R-R1)/DR)
      IF(J.GE.6)GOTO599
      GOTO(100,200,300,400,500),J
100   CONTINUE
      F=EDEN(R)*DLOG(R/B)
      GOTO1
200   CONTINUE
      V0=C*U(NN)/DSQRT(U(NN)**2+1.D0)
      F=EDEN(R)*(R*R-B*B)*V0*EPS0/R
      GOTO1
300   CONTINUE
      F=EDEN(R)*(R*R-B*B)*EPS0/R
      GOTO1
400   CONTINUE
      F=XI(NN)
      GOTO1
500   CONTINUE
      F=XI(NN)/(1.D0+U(NN)**2)
      GOTO1
599   CONTINUE
      IF(J.EQ.11)GOTO1100
      IF(J.EQ.12)GOTO1200
      F=0.D0
      IF((R.LE.R1).OR.(R.GE.R2))GOTO1
      FF=R*((R2-R)*(R-R1))**PWR
      GOTO(600,700,800,900,1000),J-5
600   CONTINUE
      F=FF
      GOTO1
700   CONTINUE
      F=FF*U(NN)
      GOTO1
800   CONTINUE
      F=FF*(U(NN)**2)
      GOTO1
900   CONTINUE
      F=FF*WOB(NN)
      GOTO1
1000  CONTINUE
      F=FF*(WOB(NN)**2)
      GOTO1
1100  CONTINUE
      F=R*XI(NN)*(WOB(NN)**2)
      GOTO1
1200  CONTINUE
      F=(R*R-B*B)*(-EPS0*EDEN(R)/R)*DM(NN)
1     RETURN
      END
      FUNCTION EDEN(R)
      INCLUDE 'ASTRONCOM.FOR'
C     CALCULATES -R*RHOD/EPS0
      EDEN=0.D0
      IF((R.LE.R1).OR.(R.GE.R2))GOTO1
      FR=(R2-R)*(R-R1)/T22
      DENS=DEN0*(FR**PWR)
      EDEN=QE*R*DENS/EPS0
```

```
1       RETURN
        ENTRY XIDLOGN(R,GAM,WOBI)
C       CALCULATES XI*DLOG(DEN)/DLOG(R)
        XIDLOGN=0.D0
        IF((R.LE.R1).OR.(R.GE.R2))GOTO2
        FR=(R2-R)*(R-R1)/T22
        F1=FR**(PWR-1.D0)
        F2=R*(R1+R2-2.D0*R)/T22
        F3=(WOB(N/2)/WOBI)**2
        F4=G00/GAM
        XIDLOGN=XI(N/2)*PWR*F1*F2*F3*F4
2       RETURN
        END
        SUBROUTINE UROOTS(UM,AAE,AAH)
C       CALCULATES ROOTS OF RADIAL FORCE BALANCE EQN
        IMPLICIT REAL*8(A-H,O-Y)
        IMPLICIT COMPLEX*16 Z
        DIMENSION A(5),R(4),Z(4)
        COMMON/CNTRL/N,DR,DR2,KBR,EPS1,EPS2,IEV
        PRINT1,AAE,AAH
1       FORMAT(' AAE= ',1PD10.3,/,' AAH= ',1PD10.3,/)
        A(1)=1.D0
        A(2)=-2.D0*AAH
        A(3)=AAH**2-AAE**2
        A(4)=0.D0
        A(5)=-AAE**2
        CALL ZRPOLY(A,4,Z,IER)
        PRINT10,Z
10      FORMAT(4(6X,1PD10.3,3X,1PD10.3,/))
C       TEST ROOTS
        NACCEPT=0
        DO100 K=1,4
        IF(DABS(DIMAG(Z(K))).GE.EPS1)GOTO100
        U=DREAL(Z(K))
        E=DABS(U*U-AAE*DSQRT(U*U+1.D0)-AAH*U)
        IF(E.GE.EPS1)GO TO100
        NACCEPT=NACCEPT+1
        PRINT20,U
20      FORMAT(6X,1PD10.3)
        R(NACCEPT)=U
100     CONTINUE
        GOTO(200,201,202,203,203),(NACCEPT+1)
200     PRINT30
30      FORMAT(//,' NO EQUILIBRIUM STATE EXISTS',//)
        STOP
201     PRINT31
31      FORMAT(//' WARNING...ONLY ONE EQUILIBRIUM STATE EXISTS',//)
        UM=R(1)
        GOTO300
202     IF(KBR.EQ.1)UM=DMAX1(R(1),R(2))
        IF(KBR.EQ.-1)UM=DMIN1(R(1),R(2))
        GOTO300
203     PRINT33,NACCEPT
33      FORMAT(//,' ERROR...',I1,' APPARENT EQUILIBRIUM STATES',//)
        STOP
300     CONTINUE
        GAM=DSQRT(UM**2+1.D0)
        EMIN=5.11D5*(GAM-1.D0)
        PRINT40,UM,GAM,EMIN
40      FORMAT(' AT R=R1:',/,'   U= ',1PD10.3,3X,'GAMMA= ',
     1  OPF8.3,3X,'EMIN= ',1PD10.3,' VOLTS',/)
        RETURN
        END
```

```
      FUNCTION UPRM(R,UU,E)
      INCLUDE 'ASTRONCOM.FOR'
      GMA=DSQRT(UU*UU+1.D0)
      GMA2=GMA**2
      WP2=QE*EDEN(R)/(EM*GMA*R)
      W0=C*UU/(GMA*R)
      W02=W0**2
      HH=QEMC2*E*R/(UU*UU*GMA)
      UPRM=(UU/R)*(1.D0-(WP2/(GMA2*W02))-GMA2*HH)/(1.D0+HH)
      RETURN
      END
      REAL*8 FUNCTION QQR(NN)
      INCLUDE 'ASTRONCOM.FOR'
      GMA=DSQRT(U(NN)**2+1.D0)
      GMA2=GMA**2
      GMA4=GMA2**2
      BETA2=1.D0-1.D0/GMA2
      H=HG(NN)/GMA
      H1=H+1.D0
      X=XI(NN)
      R=R1+DFLOAT(NN)*DR
      QQR=(1.D0-3.D0*BETA2)*(1.D0-X/GMA2-GMA2*H)/H1
     1  +(X*(3.D0/GMA2-1.D0-4.D0*BETA2*H)
     2  +H*(GMA4+4.D0*GMA2-1.D0-2.D0*BETA2*GMA4*H))
     3  /(GMA2*(H1**2))
      QQR=QQR/R
      RETURN
      END
      SUBROUTINE INPUT2
      INCLUDE 'ASTRONCOM.FOR'
      READ(15,*)
      READ(15,*)ZW,L
      EL=DFLOAT(L)
      EL2=EL**2
      READ(15,*)KT1,KT2,KT3
      DRHO1=(R1-A)/(DFLOAT(KT1)*R1)
      DRHO2=(R2-R1)/(DFLOAT(KT2)*R1)
      DRHO3=(B-R2)/(DFLOAT(KT3)*R1)
      DDRHO=DR/R1
      R2R1=R2/R1
      READ(15,*)TOL,EPS3
      READ(15,*)I2,I3
      RETURN
      END
      SUBROUTINE SHOOTER
      IMPLICIT REAL*8(A-H,O-R,T-Y)
      IMPLICIT COMPLEX*16 Z
      COMMON/GEOM/A,B,R1,R2,R2R1
      COMMON/NORM/BO1,BO12,DRHO1,DRHO2,DRHO3,DDRHO
      COMMON/CNTRL2/KT1,KT2,KT3,TOL,EPS3
      COMMON/EV/ZW,EL,EL2
      COMMON/ADMITS/ZBPLUS,ZBMINUS
      DIMENSION V(8),WW(8,9)
      EXTERNAL VFRM,STORE
      PRINT5,JIDNNT(EL)
5     FORMAT(//' EV CALCULATION: L=',I3,/)
      LL=0
      LZW=0
1     PRINT100,ZW,LZW
100   FORMAT(' ZW= ',1P2D12.4,'   ITERATION ',I2)
      IF(LL.EQ.1)GOTO200
      IF(LZW.GT.15)STOP 'EV LOOP CONVERGENCE FAILURE'
      DO10 I=1,8
```

```
10      V(1)=0.D0
        V(3)=1.D0
        RHO=A/R1
        REWIND 22
        CALL STORE(V,RHO)
        CALL STEPPER(8,V,RHO,DRHO1,RT1,TOL,WW,VPRM,STORE,100)
        ZBMINUS=-EL*DCMPLX(V(3),V(4))/DCMPLX(V(1),V(2))
        RHO=1.D0
        CALL STEPPER(8,V,RHO,DRHO2,RT2,TOL,WW,VPRM,STORE,50)
        ZBPLUS=EL*DCMPLX(V(3),V(4))/DCMPLX(V(1),V(2))
        RHO=R2R1
        CALL STEPPER(8,V,RHO,DRHO3,RT3,TOL,WW,VPRM,STORE,100)
        ZWNEW=ZW-DCMPLX(V(1),V(2))/DCMPLX(V(5),V(6))
        EREAL=DREAL(ZWNEW-ZW)/DREAL(ZW)
        EIMAG=0.D0
        IF(DABS(DIMAG(ZW)).GE.1.D-6)EIMAG=DIMAG(ZWNEW-ZW)/DIMAG(ZW)
        IF(DMAX1(DABS(EREAL),DABS(EIMAG)).LE.EPS2)LL=1
        LZW=LZW+1
        ZW=ZWNEW
        GOTO1
200     CONTINUE
        RETURN
        END
        SUBROUTINE VPRM(JX,RHO,V,DV)
        IMPLICIT REAL*8(A-H,O-R,T-Y)
        IMPLICIT COMPLEX*16 Z
        COMMON/COEF/ZMAT(4,4)
        DIMENSION V(8),DV(8)
        DIMENSION ZV(4),ZDV(4)
        DO10 J=1,4
10      ZV(J)=DCMPLX(V(2*J-1),V(2*J))
        CALL MATCAL(RHO)
        DO20 J=1,4
        ZDV(J)=0.D0
        DO30 K=1,4
30      ZDV(J)=ZDV(J)+ZMAT(J,K)*ZV(K)
20      CONTINUE
        DO40 J=1,4
        J1=2*J-1
        J2=2*J
        DV(J1)=DREAL(ZDV(J))
40      DV(J2)=DIMAG(ZDV(J))
        RETURN
        END
        SUBROUTINE MATCAL(RHO)
        INCLUDE 'ASTRONCOM.FOR'
        Y(Y1,Y2,X1,DX,X)=Y1+(Y2-Y1)*(X-X1)/DX
        IF((RHO.LE.1.D0).OR.(RHO.GE.R2R1))GOTO100
        NN1=JIDINT((RHO-1.D0)/DDRHO)
        NN2=NN1+1
        RHO1=NN1*DDRHO+1.D0
        XII=Y(XI(NN1),XI(NN2),RHO1,DDRHO,RHO)
        WOBI=Y(WOB(NN1),WOB(NN2),RHO1,DDRHO,RHO)
        UI=Y(U(NN1),U(NN2),RHO1,DDRHO,RHO)
        GAM2=1.D0+UI**2
        GAM=DSQRT(GAM2)
        BET=UI/GAM
        HGI=Y(HG(NN1),HG(NN2),RHO1,DDRHO,RHO)
        H=HGI/GAM
        PG2=1.D0+H
        ZOM=ZW-EL*WOBI
        ZOMW=ZOM/WOBI
        ZT1=1.D0+HGI**2-ZOMW**2
```

```
      ZWRC=ZW*BO1*RHO
      ZWRC2=ZWRC**2
      ZT2=ZWRC2-EL2
      ZT3=BET*ZWRC-EL
      ZDD=ZT1*ZT2+XII*ZT3**2
      ZA=ZT1/ZDD
      T=(1.DO-XII/GAM2-H*GAM2)/(1.DO+H)
      VOF=T/GAM2
      WOF=VOF-1.DO
      GAMF=T*BET**2
      HF=-XII/GAM2-H*(3.DO*GAM2-1.DO)*VOF
      XID=XIDLOGN(RHO*R1,GAM,WOBI)
      XIF=XID-XII*(GAMF+2.DO*WOF)
      ZDDF=2.DO*(GAM2*H*(GAMF*H+HF)+WOF*ZW*ZOMW/WOBI)*ZT2
     1  +2.DO*ZT1*ZWRC2+XIF*ZT3**2
     2  +2.DO*XII*ZT3*ZWRC*BET*(1.DO+VOF)
      ZDER=XID+XII*(-WOF-GAMF+HF/PG2-ZDDF/ZDD)
      ZC1=(ZOM/ZW-1.DO/GAM2)*ZDER+2.DO*XII*BET**2
      ZC=ZW*PG2*ZC1/(ZOM*ZDD)
     1  +XII*(ZT2-XII*BET**2)/(ZDD*GAM2)
     2  +1.DO
      ZDDDW=-ZOMW*ZT2/WOBI+ZT1*ZWRC2/ZW
     1  +XII*BET*BO1*RHO*ZT3
      ZDDDW=2.DO*ZDDDW/ZDD
      ZDAW=-2.DO*ZOMW/(WOBI*ZDD)-ZA*ZDDDW
      ZDDPW=2.DO*WOF*ZT2*(ZW+ZOM)/(WOBI**2)
     1  +4.DO*(GAM2*H*(GAMF*H+HF)+WOF*ZW*ZOMW/WOBI)*ZWRC2/ZW
     2  +4.DO*ZWRC2*ZT1/ZW-4.DO*ZWRC2*ZOMW/WOBI
     3  +2.DO*XIF*ZT3*BET*BO1*RHO
     4  +2.DO*XII*BET*BO1*RHO*(VOF+1.DO)*(2.DO*BET*BO1*ZW*RHO-EL)
      ZDPDW=(ZDDPW-ZDDDW*ZDDP)/ZDD
      ZDCW=-EL*WOBI*PG2*ZC1/(ZOM*ZOM*ZDD)
     1  -ZW*PG2*ZDDDW*ZC1/(ZOM*ZDD)
     2  +(ZW/ZOM)*(PG2/ZDD)*(EL*WOBI*ZDER/(ZW**2)
     3  -XII*(ZOM/ZW-1.DO/GAM2)*ZDPDW)
     4  -XII*ZDDDW*(ZT2-XII*BET**2)/(ZDD*GAM2)
     5  +XII*2.DO*ZWRC2/(ZDD*GAM2*ZW)
      GOTO200
100   CONTINUE
C     VACUUM COEFS
      ZDEL=RHO*RHO*BO12*ZW*ZW-EL2
      ZA=1.DO/ZDEL
      ZDAW=-ZA*ZA*2.DO*RHO*RHO*BO12*ZW
      ZC=1.DO
      ZDCW=0.DO
200   CONTINUE
      ZMAT(1,2)=1.DO/(ZA*RHO)
      ZMAT(2,1)=-ZC/RHO
      ZMAT(3,2)=-ZDAW/(ZA*ZA*RHO)
      ZMAT(3,4)=ZMAT(1,2)
      ZMAT(4,1)=-ZDCW/RHO
      ZMAT(4,3)=ZMAT(2,1)
      RETURN
      END
      SUBROUTINE STORE(V,RHO)
      IMPLICIT REAL*8(A-H,O-R,T-Y)
      COMMON/GEOM/A,B,R1,R2,R2R1
      COMMON/OUTS/I1,I2,I3
      DIMENSION V(8)
      IF(I2.NE.1)RETURN
      SV1=V(1)
      SV2=V(2)
      SF=RHO*R1
```

```
      WRITE(22)SR,SV1,SV2
      RETURN
      END
```

END

FILMED

9-85

DTIC